FINAL REPORT
Cooperative Agreement DE-FC02-06ER54899
SciDAC Cooperative Agreement: Center for Wave Interactions with Magnetohydrodynamics

Period 8/15/06 – 8/14/11

Submitted by the University of Wisconsin
Dalton D. Schnack, PI

The SciDAC Cooperative agreement: Center for Wave Interactions with Magnetohydrodynamics (or SWIM) was funded at the University of Wisconsin from August 15, 2006, to August 14, 2011. The only person paid directly from these funds was Dr. Thomas Jenkins, who was a post-doctoral fellow. Dr. Jenkins left UW in January, 2010, to take a job a TechX in Boulder, CO. The funds for the remaining years were subsequently transferred from UW to TechX as a subcontract. After that, all technical work performed on this Cooperative Agreement was done at TechX. The subcontract terminated on August 14, 2011, and a final report was submitted to UW.

Attached please find all progress reports submitted to USDOE by UW for the period August 15, 2006 through August 14, 2010. Also attached is the Final Report submitted by TechX to UW covering the period August 15, 2010 to August 14, 2011.

PROGRESS REPORT
Cooperative Agreement DE-FC02-06ER54899
SciDAC Cooperative Agreement: Center for Wave Interactions with Magnetohydrodynamics

Period 8/15/06 – 8/14/07

Submitted by the University of Wisconsin
Dalton D. Schnack, PI

During past year preparations we began formulation of the problem of including the effects of RF waves on low grequency MHD activity in the NIMROD code. In particular:

1. A White Paper (attached) outlining a techincal approach to the problem was prepared and distributed to the SWIM collaborators.

2. A Post-Doctoral scientist was hired to work on this problem for the next 3 years. He will begin employment in July, 2007.

The White Paper is attached.

Jan 11, 2007

On modeling the interaction of neoclassical and classical tearing modes with rf waves

C. C. Hegna, J. D. Callen, J. Carlsson, E. D. Held,
S. E. Kruger, D. Schnack, C. R. Sovinec

I. Introduction

A crucial issue for any long pulse, high temperature tokamak is the appearance of neoclassical tearing modes (NTMs). NTMs are slowly growing non-ideal MHD instabilities that produce magnetic islands at low order rational surfaces. The free-energy source for the instability is the bootstrap current which can produce islands when resistive MHD predicts stability ($\Delta' < 0$). Unlike many MHD instabilities, NTMs are metastable; they are linearly stable but nonlinearly excited at sufficient amplitude. When excited, NTMs can produce island widths that are substantial fractions of the minor radius (for β_θ values of interest to most tokamak experiments), cause significant reduction of energy confinement, and potentially lead to locked modes, loss of H-mode and/or disruption. Empirical observations indicate that the critical beta for neoclassical tearing mode onset scales with normalized ion gyroradius $\rho^*=\rho_i/a$, an extremely unfavorable scaling for most large tokamaks including ITER. Hence, methods to suppress the growth and appearance of NTMs are required. A prominent and highly successful method for NTM suppression is through the application of localized current drive in the magnetic island region. To date, the preferred tool of choice is electron cyclotron current drive (ECCD). Since various uncertainties in theoretically predicting the nonlinear island width threshold, seed island mechanisms, and the required RF suppression properties, NTM physics is one of the key MHD science questions to be addressed in a burning plasma experiment. In this document, we outline the beginnings of a program to address modeling issues of relevance to the coupled RF/MHD problem using a coupled theoretical/ computation approach.

The most commonly used paradigm for modeling NTMs is through the use of modified Rutherford equations. Such a treatment is valid if the magnetic island width exceeds the linear layer width. In this limit, the nonlinear $\boldsymbol{J}\ X\ \boldsymbol{B}$ forces overwhelm the inertia and the vicinity of the rational surface can be treated as in nearly MHD equilibrium (relative to Alfven times) and slowly evolving on the resistive diffusion time through the island region. The quasineutrality equation ($\nabla \boldsymbol{J}=0$) in the vicinity of the island in the zero pressure gradient limit ($\boldsymbol{J}_\perp=0$) is given by

$$\vec{B}\cdot\nabla\frac{J_\parallel}{B}=0,$$

which has the solution

$$\vec{J}=f(\Psi^*)\vec{B},$$

where f is a function of the helical flux surface label Ψ^*. In order to find f, resistive Ohm's law can be used

$$< \vec{E} \cdot \vec{B} >_* = \eta < \vec{J} \cdot \vec{B} >_*,$$

$$- < \frac{\partial \vec{A}}{\partial t} \cdot \vec{B} >_* = \eta < B^2 >_* f(\Psi^*),$$

where the bracket denotes an average over helical magnetic surfaces. The only surviving term from the average over the parallel electric field is due the induced electric field from the temporally growing magnetic island producing perturbation. If the island width is small relative to the minor radius, an asymptotic matching process, as used in the linear theory, can be employed. The conventional resistive-MHD prediction with zero pressure gradient leads to an island evolution equation of the form

$$\frac{dw}{dt} = \frac{\eta}{\mu_o} k_1 \Delta'$$

where w is the island width, η is the plasma resistivity, μ_o the permeability of free space, k_1 (~ 1.2) and Δ' is the asymptotic matching index. For unstable tearing modes ($\Delta' > 0$), the island width grows linearly in time and ultimately saturates due to quasilinear flattening of the current profile.

The electron viscous stress tensor modifies the Ohm's law used in fluid theory. Neoclassical theory accounts for the effect of inhomogeneous magnetic fields. In axisymmetric toroidal geometry, this leads to a damping of the electron fluid flow in the poloidal direction that ultimately produces a neoclassical modification to the Spitzer resistivity and a bootstrap current, a parallel current driven by cross field density and temperature gradients. The inclusion of neoclassical physics in Ohm's law leads to the possibility of pressure induced magnetic islands. The addition of the neoclassical modification to Ohm's law leads to a modified Rutherford equation of the form

$$\frac{dw}{dt} = \frac{\eta_{nc}}{\mu_o} k_1 [\Delta' + \Delta_{bs}(w)]$$

that produces a new term to the island evolution equation and accounts for the trapped particle correction to the plasma resistivity. In the large island limit, the new term scales as $\Delta_{bs} \sim D_{nc}/w$ with $D_{nc} \sim \varepsilon^{0.5} \beta_\theta L_q / L_p$. Essentially, this is a measure of the local bootstrap current on the helical magnetic surfaces outside the island separatrix with $L_q = q/q'$, $L_p = - p/p'$. The physics of this instability can be understood as a consequence of the self-consistent deformation of the bootstrap current profile. As the island grows, the pressure profile equilibrates along the helical field lines of the magnetic island. This leads to a helically resonant flatspot in the bootstrap current profile inside the island separatrix. This produces a magnetic resonant perturbation that is destabilizing in conventional tokamak operation with $q' > 0$. When $\Delta' < 0$, the saturated island width is given by

$$w_{sat} = \frac{D_{nc}}{(-\Delta')},$$

which can be an appreciable fraction of the minor radius.

For islands sizes smaller than the characteristic saturated value, a number of additional physical effects modify the island behavior. Diamagnetic currents,

polarization currents and ion viscous forces produce contributions. Including these effects in the quasineutrality relation gives the relation

$$\vec{B}\cdot\nabla\frac{J_{\|}}{B}=-\nabla\cdot(\frac{\vec{B}\times\nabla p}{B^2}+\frac{\vec{B}\times\rho\frac{d\vec{v}}{dt}}{B^2}+\frac{\vec{B}\times\nabla\cdot\vec{\Pi}_i}{B^2}),$$

where the ion viscous stress includes contributions from both parallel and gyrovisosity. Inverting the $\vec{B}\cdot\nabla$ operator on the lwft side yields additional parallel currents that affect island evolution. Including these effects yields a modified Rutherford equation of the form

$$\frac{dw}{dt}=\frac{\eta_{nc}}{\mu_o}k_1[\Delta'+\Delta_{bs}(w)+\Delta_{\text{int}}(w)+\Delta_{pol}(w)]$$

where the effects of resistive interchange and neoclassical polarization physics enter in through $\Delta_{int}(w)$ and $\Delta_{pol}(w)$, respectively. All of the terms on the right depend on the details of the model used; but are typically sub-dominant to the first two terms when the island is large. However, they give important corrections when the island width is small.

Of particular relevance to NTM physics is the effect of anisotropic heat flux, namely the competition between parallel and perpendicular diffusion. As mentioned previously, the NTM destabilization mechanism depends upon the self-consistent equilibration of pressure profiles along field lines. For sufficiently virulent cross-field transport (or sufficiently weak parallel transport), self-consistent flattening of the pressure profile in the island region does not occur and the neoclassical tearing instability is not active. Analysis of a temperature evolution equation with phenomenological cross-field ($\chi_\perp$) and parallel ($\chi_{||}$) heat diffusivities yields a characteristic island width ~ $(\chi_\perp/\chi_{||})^{0.25}$ below which does not allow effective pressure profile equilibration. This effect introduces a finite island width threshold. Magnetic islands that are smaller than this threshold value are not sufficiently destabilized by the bootstrap current for NTM physics to occur. Neoclassical polarization effects can also produce magnetic island thresholds, although a precise understanding of this effect is a topic of research. Crudely, the neoclassical polarization effects are important when the island width is comparable to the ion banana width. For islands below this characteristic value, the ion response is non-local and a more detailed kinetic theory needs to be worked out. Again, this is a topic of research.

In order for the NTM growth to be initiated, a magnetic island most be introduced at a level larger than the threshold value. This is referred to as the seeding problem. There are a number of theories for how seeding might occur; none of these are universally accepted as accounting for all of the experimental observations.

In an effort to combat the deleterious effects of the neoclassical tearing mode, a campaign to use localized current drive [principally electron cyclotron current drive (ECCD)] was initiated. The effect of an RF induced force on the electron fluid has principally two effects, the modification of the bulk current profile (hence effecting Δ') and the addition of a new term in the island region that alters the modified Rutherford equation.

$$\frac{dw}{dt}=\frac{\eta_{nc}}{\mu_o}k_1[\Delta'+\Delta_{bs}(w)+...+\Delta_{RF}(w)],$$

The RF term depends upon the profile of the RF source in the island region. The optimal case corresponds to an RF induced source located inside the island separatrix that essentially replaces the "missing" bootstrap current. The analytic modeling that lead to the above equation used a modified Ohm's law of the form

$$\vec{E} + \vec{v} \times \vec{B} = \eta J + ... \vec{F}_{rf}$$

with $\boldsymbol{F}_{rf} = F_{rf}(\boldsymbol{x},t)\boldsymbol{B}$. The scalar F is a prescribed function of space. While qualitative details remain to be worked out, the simple analytic modeling has compared rather favorably with the growing experimental work in this area. ECCD stabilization of NTMs has been demonstrated on a number of tokamaks and is anticipated to be the tool of choice for stabilizing NTMs in ITER.

II. Elements of simulating NTM/RF modeling

We propose a multi-level approach for simulating the interaction of an RF source with magnetic islands in a toroidal plasmas. Crudely, there are three levels of sophistication that can be pursued somewhat in parallel.

- The first approach is a computational effort somewhat paralleling the simple analytic approach to model the interaction RF with magnetic island evolution by inserting an analytically chosen form for a source term in the Ohm's law.
- In the second approach, a phenomenological evolution equation will be used to describe the temporal and spatial structure of the source term.
- In the third approach, a more rigorous analytic problem will be solved where the inclusion of RF effects are treated as closure problems. The modified equations can then be implemented in numerical simulations.

In the second and third approaches, interfaces with the RF codes will be needed.

From the discussion of the effect of RF on magnetic islands, one will note that the RF term essentially enters the modified Rutherford equation as an additional term (as it enters in Ohm's law); the RF currents do not directly affect the neoclassical drive (at least to lowest order). Hence, information on the stabilizing properties of the RF terms can also be obtained from resistive MHD calculations without neoclassical or two-effects included.

It is important that computational efforts examining the long time scale behavior of tearing instabilities be re-initiated. Prior calculations of isolated resistive MHD and neoclassical tearing modes can be revisited with the newer versions of the fluid codes. Past modeling efforts in NIMROD for studying physics centered on using a "heuristic" model for the neoclassical electron viscous stress. Efforts to improve this closure scheme as well as efforts to include two-fluid, gyroviscous, etc. effects continue as part of the CEMM project. As these advancements materialize, more sophisticated fluid treatments of magnetic island physics can be used.

a. Phenomenological model for the RF current source

The simplest way to include the effects of RF current drive in a fluid code is to add an additional term to Ohm's law,

$$\vec{E} + \vec{v} \times \vec{B} = \eta J + ... \vec{F}_{rf} = \eta(\vec{J} - \vec{J}_{rf}) + ...$$

with $\mathbf{F}_{rf} = -\eta J_{rf}(\mathbf{x},t)\mathbf{B}/B$, and the scalar J_{rf} a function to be specified. Such a calculation should allow the easiest and most direct comparison to the analytic theory described above. The crucial aspects of the current source are its amplitude, current channel width relative to the island width and the phase of the current source relative to the island phase.

b. Phenomenological evolution equation for the RF current source

At a higher level of sophistication, an evolution equation for the quantity J_{rf} can be used. One can view this approach is to include a simple RF "box" where information from the RF code enters. This approach basically models the work by Giruzzi and co-workers who used an additional evolution equation in the fluid evolution that accounts for a separate field quantity. Here, the physical effect of rapid parallel equilibration along the helical field lines is accounted for. While there are different versions of these types of models, one version is given in the form

$$\frac{\partial J_{RF}}{\partial t} + \chi_{\|}\nabla_{\|}^2 J_{rf} + \chi_{\perp}^2\nabla_{\perp}^2 J_{rf} + \nu_{rf} J_{rf} = S.$$

where the source term S is where RF codes deposit information. Due to its similarity with the temperature evolution equation, there is experience in solving equations of this form with highly disparate rates of cross-field to parallel diffusion. In steady state, rapid equilibration along field lines leads to an RF source that is distributed along the field line. Precise details for the exact nature of S and various coefficients need to be more properly defined.

An additional concern with approach is that since the above equation couples to other fluid variables, new normal modes can appear in the system. These modes could lead to unstable feedback and produce numerical instabilities. If this becomes an initial, modified or new computational approaches made need to be developed.

c. Closure scheme for modeling RF modifications to fluid equations

While the options described in the prior two sections allow for an "easy" introduction into the RF/island coupling problem, it is desirable to derive a more rigorous model for use in the simulation. The approach described here describes the problem as a closure issue. The fluid equations are evolved with the addition of extra RF sources coupled with a closure scheme modified by the RF physics.

To begin with, let's consider a kinetic equation in the form

$$\frac{df}{dt} = C(f) + Q(f),$$

where the left side is the usual kinetic operator in phase space, *C(f)* is the collision operator and *Q(f)* represents the contribution due to RF induced fields. For many applications of interest (such as ECCD), we can model *Q(f)* as a quasilinear diffusion operator of the form

$$Q(f) = \frac{\partial}{\partial \vec{v}} \cdot \vec{\vec{D}} \cdot \frac{\partial f}{\partial \vec{v}}$$

where the diffusion tensor *D* is needed from RF codes. Taking moments of our kinetic equation, we are left with the usual fluid equations augmented by additional terms from the RF source

$$\frac{\partial n_s}{\partial t} + \nabla \cdot (n_s \vec{v}_s) = 0,$$

$$m_s n_s (\frac{\partial \vec{v}_s}{\partial t} + \vec{v}_s \cdot \nabla \vec{v}_s) = n_s q_s (\vec{E} + \vec{v}_s \times \vec{B}) - \nabla p_s - \nabla \cdot \pi_s + \vec{R}_s + \vec{F}_s^{rf},$$

$$\frac{3}{2} n_s (\frac{\partial T_s}{\partial t} + \vec{v}_s \cdot \nabla T_s) + n_s T_s \nabla \cdot \vec{v}_s = -\nabla \cdot q_s - \vec{\vec{\pi}}_s : \nabla \vec{v}_s + Q_s + S_s^{rf},$$

where conventional notation is used. The additional terms due to the RF are given by

$$\vec{F}_s^{rf} = \int d^3\vec{v}\ m_s \vec{v}_s Q(f_s),$$

$$S_s^{rf} = \int d^3\vec{v}\ \frac{1}{2} m_s v_s'^2 Q(f_s),$$

with an assumption that the RF produces no particles.

$$Q(f) = \frac{\partial}{\partial \vec{v}} \cdot \vec{J}_{rf} \Rightarrow \int d^3\vec{v} Q(f) = 0,$$

and the variable **v**′ is used to denote the deviation of the phase space velocity from the fluid variable. It is important to point out that the additional RF terms appear simply as functions of three spatial dimensions and time.

At this point, the above fluid equations are exact. However, we do have to address the usual closure problem; calculations for the stress tensors and heat fluxes are needed. Since we are mostly interested in the RF modification to Ohm's law, it seems the closest analogy is with the Spitzer problem. This problem proceeds as a perturbation theory in the small quantity E/E_D where E_D is the Dreicer electric field. Since, we imagine the RF contribution is comparable to E, we assert the following balance $neE \sim F^{rf}$.

Since we are imagining the RF terms are in some sense small, we can assert that to lowest order the distribution is Maxwellian with small corrections. While this may be a poor assumption for some types of RF heated plasmas, for the case of electron cyclotron current drive, this is a good approximation. With this assertion, note that the RF contributions to the fluid equations can now be written

$$\vec{F}_s^{rf} = \int d^3\vec{v}\ m_s \vec{v}_s Q(f_s) = \int d^3\vec{v}\ m_s \vec{v}_s Q(f_{Ms})$$

$$S_s^{rf} = \int d^3\vec{v}\ \frac{1}{2} m_s v_s'^2 Q(f_s) = \int d^3\vec{v}\ \frac{1}{2} m_s v_s'^2 Q(f_{Ms})$$

to good approximation. With the identification of a proper quasilinear diffusion operator, $\boldsymbol{F}^{rf}$ and S^{rf} are now expressed as functions of low order fluid moments and RF physics.

It's important to note that with this approach, the only thing that is needed from the RF codes is the form for D as a function of the phase space variables. The procedure is the fluid code hands the state variables of interest to the RF code, the RF code subsequently determines the tensor D as a function of three spatial variables, speed, pitch angle and time and returns this information to the fluid code to determine $\boldsymbol{F}^{rf}$, S^{rf} and $Q(f)$ for use in determining the closures and fluid evolution.

Using a Chapman-Enskog-like (CEL) approach, a kinetic equation for the distortion F away from the Maxwellian is derived which can subsequently solved to obtain **q** and **π**. We write

$$f = f_M + F = n(\vec{x},t)[\frac{m_s}{2\pi T(\vec{x},t)}]^{3/2} e^{-\frac{m_s v'^2}{2T(\vec{x},t)}} + F$$

where F has no density, momentum or temperature moments. Following the usual CEL procedure where the fluid equations are used to evaluate dF_M/dt, we have

$$\frac{dF}{dt} - C(f_M + F) = ... + Q(f_M) - \frac{\vec{v}'\cdot\vec{F}^{rf}}{nT} f_M - \frac{2}{3}\frac{S^{rf}}{nT}(\frac{mv'^2}{2T} - \frac{3}{2}) f_M ,$$

where the species subscript is suppressed for simplicity. Since F is a small distortion, the collision operator on the right side can be linearized. The … bits on the right denote the "usual" CEL source terms due temperature and flow gradients that drive heat flows and viscous stresses. The important modification from the RF contribution enters as additional source terms on the right side.

To make further progress, one needs to solve the kinetic equation. Efficient and accurate solutions to equations of this form have been a topic of interest to the CEMM project (mostly through Eric Held's efforts). Solutions to the above equations should also be amendable to approaches under investigation.

As a particularly important limit, one could re-examine the equivalent Sptizer problem augmented by the RF contributions. For simplicity, let's only consider the solution along the magnetic field and further assume we are looking at time independent, homogeneous plasmas. The parallel Ohm's law (electron equation of motion) of interest is given by

$$0 \cong -neE_{\|} + R_{\|} + F_{\|}^{rf} .$$

where a number of terms/effects are dropped for simplicity. Note the closure problem for this case is due to the moment of the collision operator that has the form

$$R_{\|} = ne\eta_o J_{\|} + m_e n_e \nu_e \frac{3}{5 n_e T_e} q_{\|e} + ...,$$

with $\eta_0 = ne^2/m_e\nu_e$ (not the Spitzer resistivity). Hence $q_{||}$ (and higher order moments) require a solution to the kinetic equation. One can solve the kinetic equation using the usual prescription of expanding F in terms of Laguerre polynomials, take moments and solve the resultant matrix equation. This will lead to solutions for the higher order moments in terms of J, E, F^{rf}, etc. For the conventional Spitzer problem, it is sufficient to only go to matrices of dimension ~ three to obtain good agreement. For the problem with the RF term, it is not clear if this is the case. Further work is required.

Clearly, there are further extensions to this Spitzer-like problem that need to be addressed. These include, calculations in a bumpy cylinder, calculations in toroidal equilibrium, time-dependent processes, multiple length scale expansions, etc. Nonetheless, the closure scheme outlined above can lead to important insights as to how the more exact problem can be addressed.

III. Summary

To make progress on the problem of RF induced currents affect magnetic island evolution in toroidal plasmas, a set of research approaches are outlined. Three approaches can be addressed in parallel. These are:

- Analytically prescribed additional term in Ohm's law to model the effect of localized ECCD current drive
- Introduce an additional evolution equation for the Ohm's law source term. Establish a RF source "box" where information from the RF code couples to the fluid evolution
- Carry out a more rigorous analytic calculation treating the additional RF terms in a closure problem.

These approaches rely on the necessity of reinvigorating the computation modeling efforts of resistive and neoclassical tearing modes with present day versions of the numerical tools.

For the RF community, the relevant action item is

- RF ray tracing codes need to be modified so that general three-dimensional spatial information can be obtained.

Further, interface efforts between the two codes require work as well as an assessment as to the numerical stability properties of the procedures to be used.

CENTER FOR WAVE INTERACTIONS WITH MAGNETOHYDRODYNAMICS

Cooperative Agreement ER54899

Progress Report

Year 2

2008-2009

Submitted by:

Dalton D. Schnack

University of Wisconsin

Technical Contributions from:

Tom Jenkins, Scott Kruger, Chris Hegna, Jim Callen, Carl Sovinec, Eric Held, Fatima Ebrahimi, Johan Carlsson, Bob Harvey

The NIMROD extended MHD code[1] has been modified to include the effects of RF on MHD evolution. It has been demonstrated that a viable model for the interaction of RF (ECCD) with MHD can be constructed. The relevant details of the physics of localized ECCD deposition are captured by this model. Localized current drive induces Alfvénic disturbances along magnetic field lines, resulting in helical and spatially fluctuating current filaments at short times and a net flux-surface-averaged current on longer timescales. This average current is responsible for modifications of the matching index Δ', while the helical filaments arising at short times interfere with or enhance the helical currents associated with the tearing mode structure to influence the growth. Favorable comparisons with the results of Pletzer and Perkins[2] have been demonstrated; the optimal position for RF deposition is verified to be immediately outside the initial rational surface on which the mode grows, and the destabilizing effects induced by the shift of this surface in response to RF perturbations are correctly produced.

We believe that this work is an important step forward in the development of integrated, predictive models for ECCD/MHD interactions (such as, for example, might be used to determine optimum NTM stabilization approaches in ITER). Our model utilized toroidally symmetric ECCD deposition, with the poloidal localization of the RF fields being given essentially as an *ad hoc* function. The former assumption, though clearly not appropriate in all cases, has been used successfully to explain experimental observations[3] and is a useful approximation for plasmas undergoing rapid toroidal rotation. A more realistic model (which is a topic of ongoing research) could utilize data from ray tracing codes to determine the amplitude and spatial localization of the ECCD-induced electromotive forces. NIMROD's magnetic geometry, for instance, can be exported to the GENRAY/CQL3D [39] code[4], which can then calculate ray trajectories and power deposition associated with a particular ECCD configuration. The physics of

these coupled simulations can then be cross-checked against the conclusions of this work for consistency, and effects arising from the development of accurate closure models (which account for the effects of RF on the higher-order velocity moments) can also be compared with these results to determine the additional physics imparted by the closures. These developments, along with the rigorous verification of self-consistency among collision operators, quasilinear operators, and fluid equations, will serve as future steps of importance in the development of an integrated ECCD/MHD model.

A draft of a paper on this subject for submission to Physics of Fluids is attached.

REFERENCES

1. C. R. Sovinec, A. H. Glasser, T. A. Gianakon, D. C. Barnes, R. A. Nebel, S. E. Kruger, D. D. Schnack, S. J. Plimpton, A. Tarditi, M. S. Chu, and the NIMROD Team, J. Comp. Phys. **195**, 355 (2004).

2. A. Pletzer and F. W. Perkins, Phys. Plasmas **6**, 1589 (1999).

3. R. Prater, R. J. La Haye, J. Lohr, T. C. Luce, C. C. Petty, J. R. Ferron, D. A. Humphreys, E. J. Strait, F. W. Perkins, and R. W. Harvey, Nucl. Fusion **43**, 1128 (2003).

4. Information and documentation for GENRAY/CQL3D is available at http://www.compxco.com.

Modeling electron cyclotron current drive stabilization of resistive tearing modes in NIMROD

Thomas G. Jenkins, Carl R. Sovinec, Chris C. Hegna, and Dalton D. Schnack
Departments of Physics and Nuclear Engineering and Engineering Physics, University of Wisconsin, Madison, Wisconsin, 53706

Scott E. Kruger
Tech–X Corporation, 5621 Arapahoe Avenue Suite A, Boulder, Colorado, 80303

Abstract

A model which incorporates the effects of electron cyclotron current drive (ECCD) into the magnetohydrodynamic (MHD) equations is implemented in the NIMROD code [C. R. Sovinec *et al.*, J. Comp. Phys. **195**, 355 (2004)] and used to investigate the effect of ECCD injection on the stability, growth, and dynamical behavior of magnetic islands associated with resistive tearing modes. Predictions of the model are shown to quantitatively and qualitatively agree with numerical results obtained from the inclusion of localized ECCD deposition in static equilibrium solvers. The complete suppression of the $(2, 1)$ resistive tearing mode by ECCD is demonstrated. Consequences of the shifting of the mode rational surface in response to the injected current are explored, as are the consequences of spatial ECCD misalignment. We discuss the relevance of this work to the development of more comprehensive predictive models (in support of existing/future experiments, e.g. ITER) for ECCD–based mitigation and control of neoclassical tearing modes.

1 Introduction

Neoclassical tearing modes (NTMs) are slowly growing, metastable, nonideal magnetohydrodynamic instabilities which produce magnetic islands at low–order rational surfaces in toroidal plasmas [1, 2]. These modes arise when magnetic perturbations at such surfaces induce local flattening in the plasma pressure profile which is sufficient to depress the local bootstrap current. The modified current profile amplifies the initial perturbation, and island–shaped structures within the plasma's magnetic configuration broaden until nonlinear saturation is attained. When present, NTMs can slow plasma rotation [3], reduce core electron density and temperatures [4, 5], and possibly lead to disruption [6, 7, 8]. Various methods for their mitigation and control have been implemented in existing experiments, including the suppression of large–amplitude magnetic perturbations (e.g. sawtooth or fishbone modes) which initially excite the NTM [9, 10], or the introduction of static magnetic perturbations which interfere with mode structure [11, 12]. Of greatest relevance to this work, however, is a highly successful experimental approach involving the application of external current drive to replace the "missing" bootstrap current within magnetic islands.

In general, one can show that radio frequency (RF) waves injected into a plasma can yield localized currents (e.g. electron cyclotron current drive, hereafter ECCD) or heating (ion/electron cyclotron resonance heating, hereafter ECRH/ICRH) if these waves are suitably selected to resonate with ion or electron cyclotron motion [13]. Initial theoretical applications of this principle to the suppression and control of NTMs [14, 15] demonstrated that localized ECRH or ECCD applied at the O–point of magnetic islands could reduce island saturation widths. Subsequently, experimental results have shown [16] that the latter of these approaches more efficiently reduces the size of existing islands, and the complete stabilization of low–helicity NTMs via the application of localized ECCD within the islands has been demonstrated on several devices [17, 18, 19, 20]. Such experiments may rely on sophisticated active feedback control to locate and drive time–modulated current in island O–points of the rotating plasma [10, 12, 21, 22, 23], or may continuously drive current whose spatial alignment is tailored to yield a net stabilizing effect on the NTM [24]. Considerable efforts have been made to determine an optimal strategy for NTM mitigation and control in the ITER device [15, 21, 25, 26] utilizing these two approaches.

Although efforts to suppress and/or control NTMs in existing experiments have met with notable success, the development of predictive computational models to simulate the interaction of MHD with ECCD and other forms of RF remains a significant challenge [27]. In part, this is due to the disparity in the relevant timescales; the Alfvén time characterizing MHD phenomena may vary by orders of magnitude from both the more rapid electron cyclotron period and the slower resistive timescales associated with NTMs. Further complexities include the calculation of self–consistent propagation trajectories of RF waves as they pass through the plasma's magnetic geometry — which may be perturbed by the growth of islands — as well as the accurate calculation of RF–modified heat transport and its effect on the pressure profile and bootstrap current [28]. In addition, the internal consistency of the bounce–averaged Fokker–Planck RF operator with the collision operator and the kinetic equation (from which fluid moments are derived) must be ensured; the latter two entities involve distribution functions of three spatial and three velocity–space coordinates, while the Fokker–Planck operator is a function of only one spatial and two velocity–space coordinates [29] in the low–collisionality regime of interest. Finally, the effects of RF energy and momentum transfer to the plasma must be included in the calculation of numerically viable neoclassical closures for the MHD equations.

While recent work on various aspects of the ECCD/MHD coupling problem appears promising (e.g., in the development of closures [30], theoretical foundations [31], and self–consistent forms of the fluid equations and the collision/RF operators [32, 33]), we choose to direct the focus of this work toward a more elementary question — how will an externally imposed electromotive force in the MHD Ohm's law influence the behavior of magnetic islands? It can be demonstrated (see Appendix A) that the dominant term in a coupled ECCD/MHD model appears in this form in the Ohm's law. We show that the resultant system of equations, though not fully self–consistent, demonstrates the basic physical

principles associated with this particular RF/MHD coupling, agrees quantitatively and qualitatively with the work of other authors, and provides insight applicable to the development of more comprehensive simulation models for the mitigation and control of NTMs [27].

Section II of this paper presents equations which model the coupling of ECCD with MHD, and shows that the study of *resistive* (rather than neoclassical) tearing modes allows the exploration of physics issues relevant to this coupling. An analytic example is presented in simple geometry which demonstrates the physical effects induced by RF deposition, and the persistence of these effects in toroidal geometry is demonstrated. In section III, we implement the model of ECCD/MHD coupling in the NIMROD code [34, 35] and consider the long–time effects of localized current deposition on the stability properties of the plasma equilibrium. We show that complete suppression of the (2,1) resistive tearing mode can be achieved through adequate alignment of the ECCD. Physical consequences associated with the shifting of the mode rational surface in response to localized current drive are also considered, and the need for accurate radial alignment of the induced current (discussed experimentally by Ref. [21]) is demonstrated. Section IV discusses the response of the plasma to ECCD deposition on shorter timescales; the growth of resistive tearing modes is shown to have significant variability in response to the transient phenomena induced by the current drive. Finally, section V summarizes key results and discusses the relevance of this simulation model to the more general problem of simulating ECCD stabilization of NTMs.

2 The coupled ECCD/MHD model

In this work the RF–modified MHD equations take the form

$$\nabla \cdot \mathbf{B} = 0 \tag{1}$$

$$\nabla \times \mathbf{B} = \mu_0 \mathbf{J} \tag{2}$$

$$\nabla \times \mathbf{E} = -\frac{\partial \mathbf{B}}{\partial t} \tag{3}$$

$$\frac{\partial \rho}{\partial t} + \nabla \cdot [\rho \mathbf{u}] = 0 \tag{4}$$

$$\rho \frac{\partial \mathbf{u}}{\partial t} + \rho(\mathbf{u} \cdot \nabla)\mathbf{u} = -\nabla p + \mathbf{J} \times \mathbf{B} - \nabla \cdot \overleftrightarrow{\mathbf{\Pi}} \tag{5}$$

$$\mathbf{E} + \mathbf{u} \times \mathbf{B} = \eta \mathbf{J} + \frac{\mathbf{F}_e^{rf}}{n|q_e|} \tag{6}$$

$$\frac{3}{2} n \left(\frac{\partial T}{\partial t} + (\mathbf{u} \cdot \nabla) T \right) + p \nabla \cdot \mathbf{u} = -\nabla \cdot \mathbf{q} - \overleftrightarrow{\mathbf{\Pi}} : \nabla \mathbf{u} + Q \ ; \tag{7}$$

the origins of the various terms are summarized in Appendix A and the references therein. Here, the electric and magnetic fields $\mathbf{E}$ and $\mathbf{B}$ vary as functions

of both space and time, as do the mass density, velocity, current, pressure, and temperature ($\rho, \mathbf{u}, \mathbf{J}, p$, and T) associated with the conducting fluid of the MHD model. The quantities μ_0 and η respectively represent the vacuum permeability and the plasma resistivity, while the heat flux $\mathbf{q}$ and the anisotropic stress tensor $\mathbf{\Pi}$ are associated with the closure schemes discussed in Appendix A. The final term in Eq. (6) is nonstandard and models the ECCD interactions with the plasma. It can be envisioned as an electromotive force induced by the RF on the conducting fluid. In this work we will stipulate that this term has the form

$$\frac{\mathbf{F}_e^{rf}}{n|q_e|} = -\frac{\eta\lambda\mathbf{B}f(\mathbf{x},t)}{\mu_0} \ . \tag{8}$$

where λ has units of inverse length and is associated with the ECCD amplitude, while $f(\mathbf{x},t)$ is a dimensionless function stipulating the spatial and temporal localization of RF deposition. This form is physically reasonable, as one expects the induced emf to induce current parallel to magnetic field lines on the resistive timescale $\tau_R \sim \mu_0/\eta$. A simple analytic model can be constructed to verify this effect and explore its consequences.

2.1 Plasma response — cylindrical model

Consider a plasma bounded by a cylindrical domain of radius a which is periodic in length L. Neglecting stresses, heat fluxes, and collisional heating ($\mathbf{q}, \mathbf{\Pi}, Q$) in Eqs. (1 – 7) for simplicity, and in the absence of RF, it is easy to show that an equilibrium with constant magnetic field $\mathbf{B}_0 = B_0\hat{z}$, pressure $p_0 = n_0T_0$, and density ρ_0 exists, with zero equilibrium velocity $\mathbf{u}_0$, electric field $\mathbf{E}_0$, current $\mathbf{J}_0$, and RF injection $f_0(\mathbf{x},t)$. In this section, equilibrium and perturbed quantities will be subscripted with zeros and ones respectively [with the exception of the subscripts denoting the order of the Bessel functions $J_0(x)$ and $J_1(x)$, which may appear in either equilibrium or perturbed quantities but will always be preceded by the symbol J]. Now suppose that an RF perturbation is abruptly introduced into this equilibrium, with $f_1(\mathbf{x},t)$ taking the form

$$f_1(\mathbf{x},t) = \eta(t)J_0\left(\frac{r\alpha_{1,0}}{a}\right)\left[K_1 + K_2\cos(kz)\right] \ . \tag{9}$$

Here $\eta(t)$ is the unit step function, $k \equiv 2\pi/L$, J_0 is the aforementioned Bessel function of order zero (whose pth zero is given by $\alpha_{p,0}$), and K_1, K_2 are constant. This form is chosen because the equilibrium "flux surfaces" in this problem are individual field lines in the $\hat{z}$ direction; the physics of interest is the plasma's response as the RF induces current within a flux surface parallel to the field. Explicitly defining a flux–surface averaging operator

$$\langle\bullet\rangle \equiv \frac{1}{L}\int_0^L \bullet \, dz \ , \tag{10}$$

one may denote the fluctuation as $\delta f_1 = f_1 - \langle f_1\rangle$ and observe that the z–independent component of f_1 (the K_1 piece) represents its flux–surface average,

while the $\cos(kz)$ component (K_2 piece) represents a spatial fluctuation about this average. We will demonstrate that the responses of the plasma to the RF's flux–surface averaged component $\langle f_1 \rangle$ and fluctuating component δf_1 differ in important ways.

Linearizing Eqs. (1 – 7) and using Fourier–Laplace transforms, it can be shown that the perturbed density and pressure are zero, while the other perturbed quantities are given by

$$\mathbf{B}_1 = B_0 \eta(t) J_1(x) \frac{\lambda a}{\alpha} \left(K_1 (1 - e^{-\gamma t}) + \frac{K_2 \gamma}{\omega} e^{-\Omega t} \cos(kz) \sin(\omega t) \right) \hat{\theta} \quad (11)$$

$$\mathbf{u}_1 = v_A \frac{\eta(t)}{S} J_1(x) \frac{\lambda \alpha}{k} K_2 \sin(kz) \left[e^{-\Omega t} \left(\cos(\omega t) + \frac{\Omega}{\omega} \sin(\omega t) \right) - 1 \right] \hat{\theta} \quad (12)$$

$$\mathbf{E}_1 = v_A B_0 \frac{\eta(t)}{S} J_1(x) \frac{\lambda \alpha}{k} K_2 \sin(kz) \cdot \quad (13)$$

$$\left[1 - e^{-\Omega t} \cos(\omega t) + \left(\frac{\Omega - \gamma}{\omega} \right) e^{-\Omega t} \sin(\omega t) \right] \hat{r} \quad (14)$$

$$- \quad v_A B_0 \frac{\eta(t)}{S} J_0(x) \lambda a \cdot \quad (15)$$

$$\left[K_1 e^{-\gamma t} + K_2 \cos(kz) \left(1 - \frac{\gamma}{\omega} e^{-\Omega t} \sin(\omega t) \right) \right] \hat{z} \quad (16)$$

$$\mathbf{J}_1 = \frac{B_0}{\mu_0} \eta(t) J_1(x) \frac{\gamma \lambda k a}{\omega \alpha} K_2 \sin(kz) e^{-\Omega t} \sin(\omega t) \hat{r} \quad (17)$$

$$+ \quad \frac{B_0}{\mu_0} \eta(t) J_0(x) \lambda \left(K_1 (1 - e^{-\gamma t}) + \frac{K_2 \gamma}{\omega} e^{-\Omega t} \cos(kz) \sin(\omega t) \right) \hat{z} \quad (18)$$

wherein $v_A \equiv B_0/(\mu_0 \rho_0)^{1/2}$ is the Alfvén velocity, $S \equiv \tau_R/\tau_A$ is the Lundquist number [with $\tau_A \equiv a/v_A$ being the Alfvén time and $\tau_R \equiv \mu_0 a^2/\eta \gg \tau_A$ the resistive diffusion time], $\alpha = \alpha_{1,0}$, $x \equiv r\alpha/a$, and we have introduced the quantities (each with units of inverse time)

$$\Omega \equiv \frac{\alpha^2 + k^2 a^2}{2\tau_R} \quad (19)$$

$$\omega \equiv (k^2 v_A^2 - \Omega^2)^{1/2} \quad (20)$$

$$\gamma \equiv \frac{\alpha^2}{\tau_R} \, . \quad (21)$$

Now consider the component of the linearized Ohm's law, Eq. (6), which is parallel to the equilibrium field $\mathbf{B}_0 = B_0 \hat{z}$ and given by

$$E_{1z} = \eta J_{1z} - \frac{\eta \lambda B_0 f_1}{\mu_0} \, . \quad (22)$$

Using the flux–surface averaging operator, we can explicitly write the averaged ($\sim K_1$; z–independent) and fluctuating ($\sim K_2$; z–dependent) pieces of this equation as

$$\underbrace{-v_A B_0 \frac{\eta(t)}{S} J_0(x)\lambda a e^{-\gamma t}}_{\langle E_\parallel \rangle} = \eta \underbrace{\frac{B_0}{\mu_0}\eta(t) J_0(x)\lambda \left(1 - e^{-\gamma t}\right)}_{\langle J_\parallel \rangle} - \frac{\eta\lambda B_0}{\mu_0} \underbrace{\eta(t) J_0(x)}_{\langle f \rangle} \ , \quad (23)$$

$$\underbrace{-v_A B_0 \frac{\eta(t)}{S} J_0(x)\lambda a \cos(kz) \left(1 - \frac{\gamma}{\omega} e^{-\Omega t} \sin(\omega t)\right)}_{\delta E_\parallel} =$$

$$\eta \underbrace{\frac{B_0}{\mu_0}\eta(t) J_0(x)\lambda \frac{\gamma}{\omega} e^{-\Omega t} \cos(kz) \sin(\omega t)}_{\delta J_\parallel} - \frac{\eta\lambda B_0}{\mu_0} \underbrace{\eta(t) J_0(x) \cos(kz)}_{\delta f} \ , \quad (24)$$

wherein K_1 and K_2 have been dropped for conciseness in the respective equations. Consider Eq. (24), the fluctuating parallel Ohm's law. As the RF abruptly turns on, z–dependent electric fields are immediately induced to counter its effects. Shear Alfvén waves are also launched along the equilibrium field lines; these waves are associated with fluctuating parallel currents and electric fields in this geometry ($\omega \sim k v_A$ since $S \gg 1$). These waves gradually damp away on the the resistive timescale, leaving only the original, spatially varying parallel electric fields to smooth away the spatially varying electromotive forces imparted by the RF.

The flux–surface averaged parallel Ohm's law, Eq. (23), behaves differently. Initially, z–independent electric fields also arise to counter the RF electromotive forces [as was the case in Eq. (24)]. However, rather than persisting at long times, these fields subsequently decay on the resistive timescale. As they do so, a flux–surface averaged parallel current flow — the "driven current" referred to in the ECCD acronym — arises to preserve the relationship in the parallel Ohm's law.

From this, a number of important general conclusions may be drawn about the linear behavior of the plasma in response to the newly–added RF term in Ohm's law. In the long–time limit of many resistive diffusion times,

> (a) current flow parallel to the equilibrium magnetic field lines is induced, with amplitude proportional to the flux–surface average of the RF drive; and
>
> (b) static parallel electric fields are induced to smooth RF–induced spatial variation about this average.

At short times, however,

> (c) parallel electric field is induced in response to the flux–surface averaged component of the RF drive, while
>
> (d) spatial variations about this average are smoothed both by induced parallel electric fields and Alfvénic currents, both of which vary rapidly in time.

In toroidal geometry, wherein general plasma equilibria cannot be written in explicit analytic forms, the physical effects of the RF drive can nevertheless be determined by the principles above. Toroidal magnetic equilibria can be characterized by the safety factor $q(\psi)$, a flux–surface function expressing the ratio of toroidal to poloidal transits of the device experienced by a closed field line on that flux surface. On rational surfaces, the value of $q(\psi)$ is a ratio of small integers; a given field line closes on itself after a relatively small number of toroidal transits of the device. It is these surfaces on which tearing modes arise and near which RF deposition is desirable to counter them. RF–induced current drive which intercepts field lines on rational surfaces will, according to the principles above, launch co– and counter–propagating Alfvén waves along helical field line paths. On a timescale much shorter than the resistive time, these waves will meet at the point opposite their launch point on the helix and nonlinearly beat together (an effect ignored in our analytic model). However, as these waves are associated with the (helical) equilibrium field line, and the resistive diffusion time is slow, the structure of the resulting current perturbation remains helical.

Using the NIMROD code, this helical structure can be simulated. In Figure 1 a computational grid and an axisymmetric equilibrium profile for the parallel current $\mu \equiv \mu_0 \mathbf{J}\cdot\mathbf{B}/B^2$ (which monotonically decreases toward the plasma edge) are shown for a typical tokamak geometry. NIMROD uses a finite element representation in the poloidal plane, enabling grid packing about the $q = 2$ and $q = 3$ rational surfaces; q is monotonically increasing toward the plasma edge and will be shown in Figure 3a. We restrict the RF source term to a be narrow Gaussian function in the poloidal plane (centered at the $q = 2$ surface on the outboard midplane) and to span only one–tenth of the tokamak's toroidal extent. We then evolve the MHD equations over several thousand Alfvén times and examine the resultant modifications to the μ profile. Figure 2 demonstrates that the profile perturbations (obtained by subtracting off the axisymmetric equilibrium of Figure 1 from the total profile) indeed have a helical structure consistent with the localization of the RF near the $q = 2$ surface; poloidal cross–sections separated by π radians in the toroidal angle contain μ profiles whose maxima are rotated by $\pi/2$ radians relative to one another.

On nonrational surfaces, which are covered ergodically by a single field line, localized RF deposition also excites Alfvén waves propagating in both directions along field lines intercepting the deposition region. The timescale on which nonlinear wave beating occurs varies considerably in this case; waves may make relatively few or relatively many transits of the device [depending on the local value of $q(\psi)$] before meeting up with their oppositely–directed counterparts. Because this disparity between deposition at rational and nonrational surfaces potentially introduces a broad range of timescales, the studies of short– and long–time effects of ECCD deposition presented hereafter in this work use sources which are toroidally symmetric. In this case, the "helical" current perturbations associated with the deposition exhibit the same toroidal symmetry as their launch points, and nonlinear wave beating occurs on the same timescale for both rational and nonrational surfaces. This approach enables one

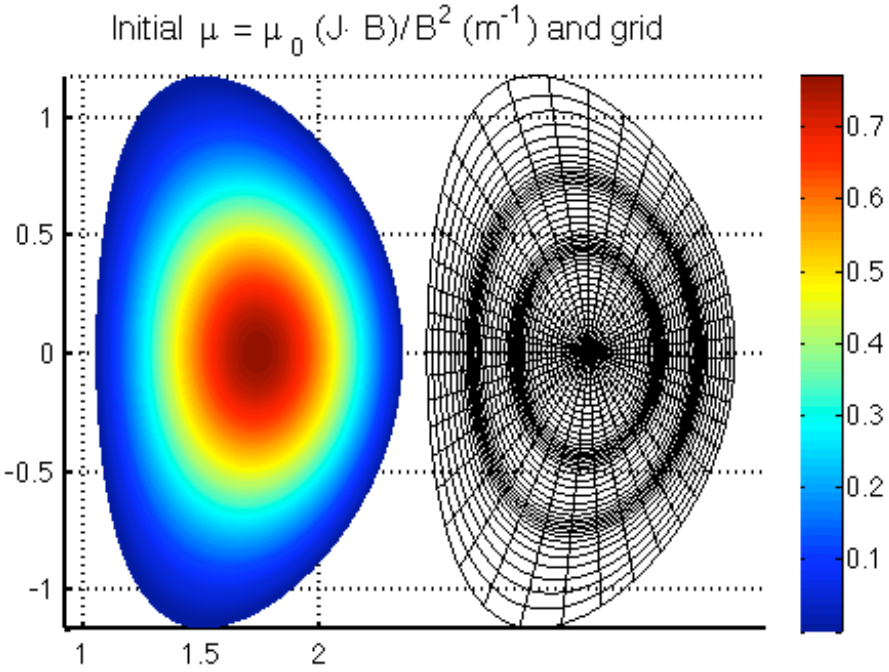

Figure 1: The axisymmetric, equilibrium parallel current profile $\mu = \mu_0(\mathbf{J} \cdot \mathbf{B})/(\mathbf{B} \cdot \mathbf{B})$ for a toroidal plasma, along with the finite element mesh used to simulate the evolution of the RF/MHD equations in the NIMROD code. (For clarity, only every third gridline is shown in the mesh.) The simulations utilize mesh packing about the $q = 2$ (inner) and $q = 3$ (outer) rational surfaces.

to classify short– and long–time effects of ECCD deposition in the context of the Rutherford equation for island growth, which we now discuss.

2.2 The Rutherford equation

The growth of magnetic islands generated by tearing modes in tokamaks can be described heuristically by a Rutherford equation [36], appropriately modified to include the neoclassical effects associated with toroidal geometry. Such an equation can be written (following Ref. [37]) in the form

$$\frac{dw}{dt} = \frac{\rho_s^2}{\tau_R}(\Delta' + \Delta'_{bs} + \Delta'_{curv} + \Delta'_{pol} + \Delta'_{ECCD} + \Delta'_H) \tag{25}$$

In this equation, w is the width of the magnetic island, ρ_s is the value of the radial coordinate ρ (in the toroidal geometry) at the rational surface, and $\tau_R \equiv a^2\mu_0/\eta$ is the conventional resistive diffusion time of the plasma (with a

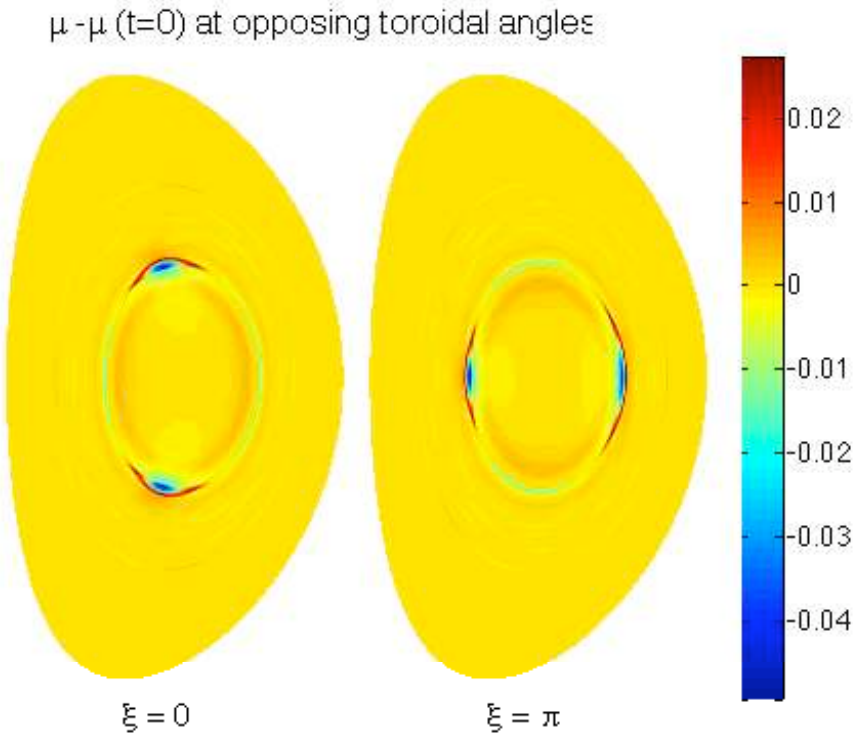

Figure 2: In the presence of a poloidally and toroidally localized RF source, helical perturbations to the μ profile of Figure 1 arise as the MHD equations are evolved forward in time. Here, the RF is deposited in a narrow Gaussian peak on the $q = 2$ surface at the outboard midplane. Toroidally, the RF is bounded to span only one–tenth of the toroidal coordinate ξ; Alfvén waves are launched along the magnetic field lines intercepted by the RF deposition.

now a representative scale length on the order of the minor radius). The matching index Δ' is the fundamental parameter associated with resistive tearing modes; it measures the discontinuity in the radial logarithmic derivative of the poloidal flux at the rational surface (quantifying the free energy attainable by reconnective alteration of the magnetic topology). The subscripted Δ' quantities represent the contribution of various RF and neoclassical effects (bootstrap current destabilization, curvature and polarization current stabilization, and the effects of ECCD injection and heating from ECRH) to the island evolution. The detailed form of the majority of these terms will be unimportant for this work, but the method by which the terms *enter* the Rutherford equation — namely, as additive corrections to the original Δ' term — is important. It implies that the physics underlying the ECCD/MHD interaction is *independent* of neoclas-

sical effects. The neglect of these effects, and the complicated closure schemes associated with them, greatly simplifies numerical simulations.

After dropping the term related to resonance heating (in keeping with the assumptions in Appendix A), a representative Rutherford equation for the study of ECCD effects in MHD is given by

$$\frac{dw}{dt} = \frac{\rho_s^2}{\tau_R}[\Delta' + \Delta'_{ECCD}] \ . \tag{26}$$

Though we do not explicitly solve this equation, its components can be associated with the physical effects demonstrated in section 2.1. The matching index Δ' can be determined from the (toroidally symmetric) magnetic equilibrium. It has a constant value on any particular flux surface, from which the stability properties of the equilibrium (in the absence of RF) may be deduced. Consequently, only the flux–surface averaged component of the injected ECCD — which arises at long times — can influence its value. For initially unstable equilibria, the Δ_{ECCD} term must therefore capture physics relevant to interactions of the growing mode with the helical, short–time, transient perturbations induced by the ECCD. It should be noted here that the metastability associated with neoclassical tearing modes is not present in this model; though the short–time fluctuations associated with ECCD injection may induce tearing mode–like structures in initially stable equilibria, the long–time behavior of the system will be determined by the matching index Δ'.

The remainder of this work will focus on the influence of the parameters characterizing our RF deposition model on the growth rates of resistive tearing modes. We consider these effects both at the long timescales associated with Δ' modification and the short timescales associated with the Δ'_{ECCD} term of Eq. (26).

3 Effects of ECCD deposition on resistive tearing modes — the long–time limit

As previously noted, the initial linear behavior of resistive tearing modes is governed by the matching index Δ', which depends only on the properties of the plasma equilibrium. When the matching index is adequately large (> 0 in the case of resistive tearing modes) on a particular rational surface, reconnection occurs and magnetic islands are formed; the current perturbations associated with the island exhibit the same helicity as the field lines of the rational surface. Initially, the island widths increase exponentially; however, nonlinearly driven eddy currents soon begin to supersede the role of plasma inertia in the island growth, leading to slower growth which is algebraic in time [36]. Ultimately, a saturated state — a fixed island width — is attained, as the free energy obtainable from additional rearrangement of the magnetic topology (via additional helical current flow) becomes comparable with the energy required to accomodate this new topology (i.e., to bend field lines outside the island; see [38]). We

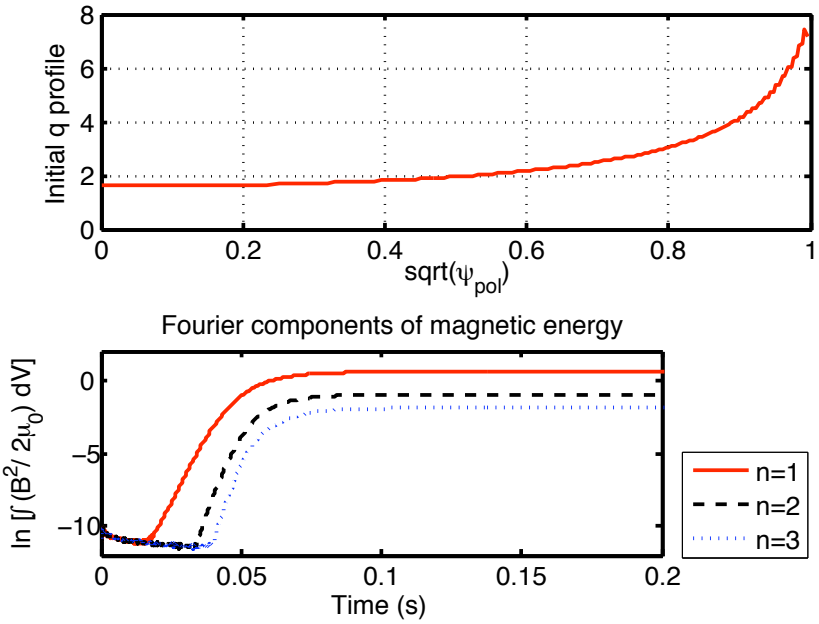

Figure 3: (a) The initial q profile for the toroidal plasmas considered in this work. The equilibrium is unstable to $(m, n) = (2, 1)$ tearing modes, which occur at the $q = 2$ rational surface (initially located at $\sqrt{\psi_{pol}} = 0.525$). (b) The growth of various Fourier components (corresponding to variation in toroidal angle ξ) of the volume–averaged magnetic energy as the MHD equations are evolved in time. The $n = 1$ component predominates, initially growing exponentially and then saturating. (Note that other tearing modes are also present, but the amplitudes of these modes are comparatively small.)

demonstrate the simulation of this mode in NIMROD in Figure 3b; RF effects are not included in this simulation. The growth of the $n = 1$ Fourier component of the magnetic energy (associated with the helical structure of the magnetic field perturbations in the island) is initially exponential, but is followed by a period of slower growth and saturation. Hence, in the absence of RF, the initial growth of the islands is dictated by the toroidally symmetric equilibrium profiles, while their ultimate width is governed by helical perturbed currents.

Because the resistive tearing mode obtains its free energy from current profile gradients, the toroidally averaged, normalized parallel current profile μ is a useful diagnostic of its behavior. In Figure 4 we demonstrate this effect; on average, the initial μ profile (monotonically decreasing toward the plasma edge) undergoes a net flattening due to current perturbations near the $q = 2$ rational surface (positioned at the cross in the lower portion of the figure) as the tearing mode grows and saturates. Hence, the flattening of the profile near the rational

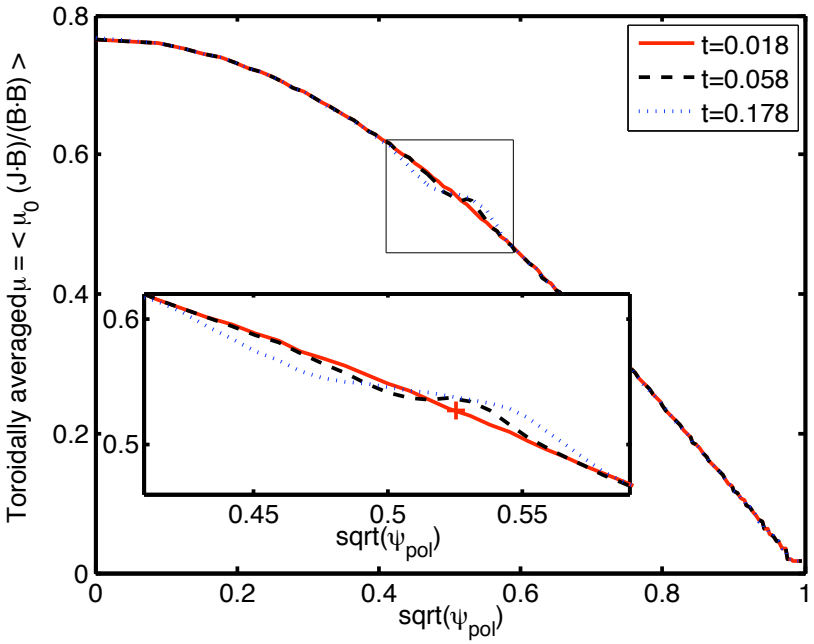

Figure 4: Time evolution of the toroidally–averaged μ profile in the absence of ECCD. The rational surface from which the tearing mode grows is initially located at $\sqrt{\psi_{pol}} = 0.525$. (inset) Close–up of the toroidally–averaged μ profile as the tearing mode grows and saturates (compare with Figure 3b). The position of the rational surface is denoted by a cross; as the mode saturates, a local flattening of the μ profile is observed near this point.

surface can be associated with stability, and additional stabilizing or destabilizing contributions may result from RF–induced current perturbations which locally flatten or steepen this profile.

The modification of Δ' by the ECCD is particularly easy to simulate using the NIMROD code [34]. Relative to a known toroidal equilibrium, NIMROD uses a high–order finite element representation to describe perturbed physical quantities in the poloidal plane and a bounded Fourier representation to describe the variation of these quantities with respect to toroidal angle. One may consequently express an arbitrary perturbed physical quantity (e.g., pressure, field components, etc.) in the form

$$\delta A(R, Z, \xi, t) = \sum_{n=-N}^{N} \delta A_n(R, Z, t) e^{in\xi} \ ; \tag{27}$$

the toroidally symmetric perturbations induced by the RF can thus be constructed by initially evolving only the $n = 0$ components of the MHD equations

(1)–(7) forward in time. This approach preserves axisymmetry while suppressing the growth of tearing modes, which depend on helical perturbations. It is conveniently compatible with the earlier stipulation that the RF perturbation exhibit toroidal symmetry (to avoid discrepancies between currents driven on rational and nonrational surfaces). The ECCD deposition must approach some time–independent steady state if the long–term modification of Δ' is to be determined. Consequently, the simulations in the remainder of this work use an ECCD model [following Eq. (8)] with

$$f(\mathbf{x},t) = \exp\left(-\frac{(R-R_{rf})^2+(Z-Z_{rf})^2}{w_{rf}^2}\right) g(t) \tag{28}$$

with

$$g(t) = \left[\frac{1}{2}\tanh\left(\frac{t-t_o}{t_p}\right) + \frac{1}{2}\tanh\left(\frac{t_o}{t_p}\right)\right] \ . \tag{29}$$

Subscripted quantities in Eqs. (28 – 29) are simulation parameters, with w_{rf} denoting the characteristic width ("spotsize") about a central deposition point (R_{rf}, Z_{rf}). Following an offset t_o, the time–dependent term ramps up from zero to asymptotically approach unity on a timescale $t_p \approx \tau_R$.

Our simulations proceed as follows: beginning with an equilibrium state which is stable to ideal MHD perturbations and unstable to the $(m,n) = (2,1)$ resistive tearing mode, we evolve the axisymmetric Fourier components of the MHD equations in response to ECCD injection of the form (28) – (29). After several resistive times, the perturbations induced by the RF relax to a time–independent state, yielding a modified equilibrium. Toroidally asymmetric Fourier components of the MHD equations are then permitted to evolve, enabling the growth of the tearing mode. Because the mode growth rate is proportional to some near–unity power of Δ', comparison of the growth rate in the presence or absence of RF reveals the influence of the applied RF on the mode stability. In essence, this approach uses NIMROD's dynamical modeling capability to address questions very similar to those posed by Pletzer and Perkins [24], who used the (static) code PEST-3 to calculate Δ' modifications due to toroidally symmetric, poloidally Gaussian current profiles injected at or near the mode rational surface.

As noted in the aforecited work by Pletzer and Perkins, one primary effect of RF–induced currents is to modify the position of this rational surface; perturbed currents yield perturbed magnetic fields and q profiles. We explore this effect explicitly in Figure 5, wherein the ECCD profiles of the above procedure are Gaussian and have half–width $w_{rf} = 0.037$ m. The injection is centered about equally spaced radial coordinates on the outboard midplane ($Z_{rf} = 0$). The ECCD amplitudes λ for the various datapoints are chosen such that the ratio of ECCD–induced toroidal current to initial toroidal current (from the equilibrium configuration) ranges from 1–4%. One can estimate the percentage P of the RF which is deposited inboard from the original position $R_{2,1}(= 2.027$ m) of the rational surface by integrating Eq. (28) over all Z and all $R < R_{2,1}$ to obtain

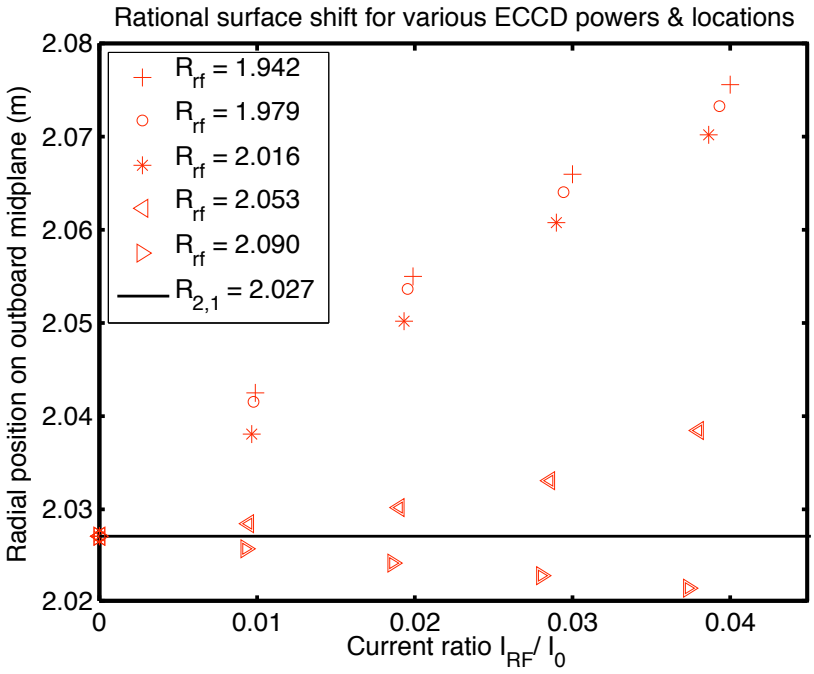

Figure 5: Shift of the position of the $q = 2$ rational surface in response to ECCD deposition peaking at various amplitudes and locations. All radial coordinates lie on the outboard midplane. The solid line denotes the original position $R_{2,1}$ of the rational surface. Radial outward shifts are induced by deposition centered inboard from (and even slightly outboard from) this surface; such shifts must be accounted for in determining optimal ECCD alignment. The ECCD deposition is Gaussian with half–width $w_{rf} = 0.037$.

the result $P = 0.5 + 0.5\ \mathrm{erf}[(R_{2,1} - R_{rf})/w_{rf}]$. Outward shifts of the $q = 2$ surface arise even when upwards of 80% of the RF deposition occurs outside the initial rational surface; the latter result is consistent with Figure 2 in the treatment by Pletzer and Perkins [24].

La Haye [21] has noted the critical need for accurate spatial alignment of RF deposition for the mitigation and control of NTMs, and examination of the modified growth rates which result from ECCD–induced alterations of Δ' at long times in our model also affirm the need for accurate spatial alignment of the RF. In Figure 6, we show the growth rates for various values of the RF amplitude parameter λ when RF is applied at the deposition points noted above (the poloidal spotsize remains at $w_{rf} = 0.037$ m). Relatively minor modifications to the growth rate occur for RF deposition which is misaligned with the rational surface (see, e.g., the "+" or ">" markers in the plot), indicating that RF deposition is a highly inefficient stabilization mechanism for large misalign-

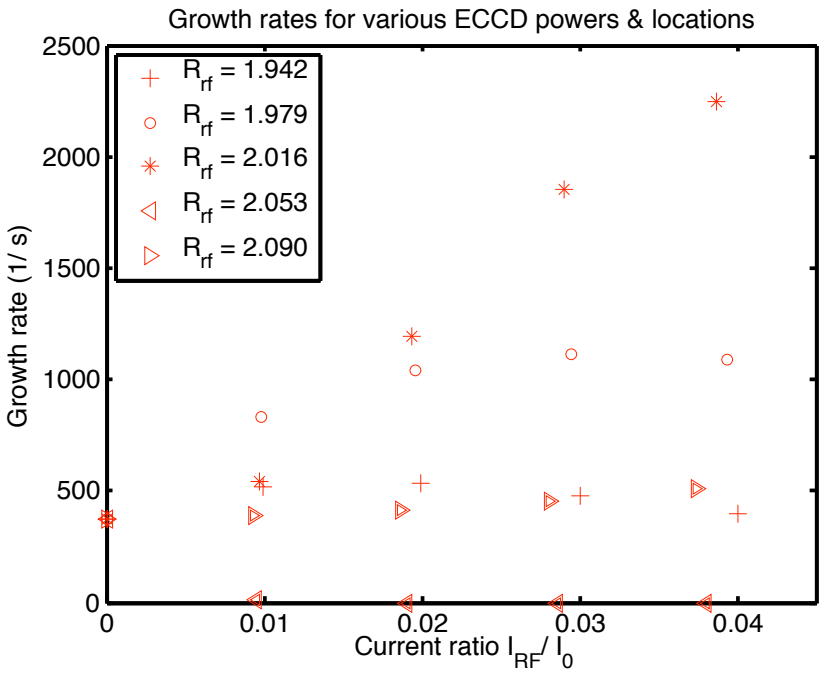

Figure 6: Modified linear growth rates of the $(2,1)$ tearing mode as ECCD is deposited on the plasma outboard midplane. The ECCD drives toroidal current whose steady–state value, relative to the equilibrium toroidal current, determines the current ratio; the initial position of the rational surface on the outboard midplane is at $r = 2.027$ m. Deposition far from the rational surface has relatively little influence on the growth rate, while significant destabilizing effects on mode growth are caused by deposition near the rational surface on the inboard side. The mode can be stabilized completely for large current ratios if ECCD deposition occurs near the rational surface on the outboard side.

ments with the rational surface. More notable effects occur when the peak RF deposition occurs just inside the rational surface (the "o" and "$*$" markers) or just outside this surface (the "$<$" markers). In the former cases, the growth rate of the tearing modes is significantly *increased*; the current profile of the plasma has been altered in a destabilizing manner (an obviously undesirable effect). In the latter case, however, the deposition of RF just outside the rational surface completely stabilizes the tearing mode at long times. These results are also consistent with Figure 6 in the work by Pletzer and Perkins, wherein highly localized Gaussian current perturbations ($\sigma = 0.03$, in their notation) cause significant destabilizing effects inside the rational surface but are stabilizing outside.

Because the ultimate influence of the ECCD on islands generated by resis-

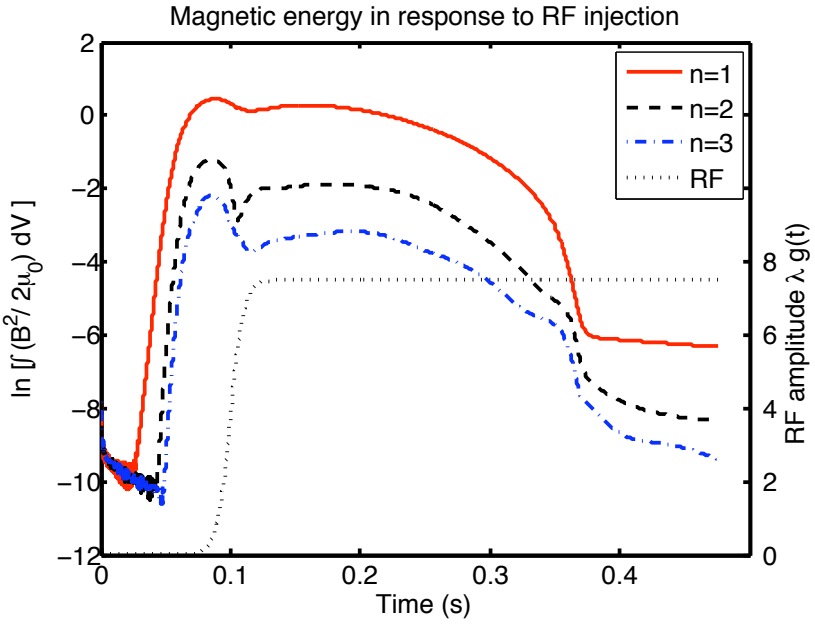

Figure 7: Low–order Fourier components of the volume–integrated magnetic energy for an equilibrium unstable to the (2,1) resistive tearing mode. ECCD injection appropriately applied on the outboard midplane yields a slow, but increasingly rapid, reduction in the $n = 1$ magnetic energy as the discharge evolves. This reduction is associated with the reduction of the width of magnetic islands since $E_{mag} \sim w^4$). Complete stabilization of the mode is achieved by $t \approx 0.38$ s.

tive tearing is governed by its long–time effects on the Δ' term of Eq. (26), the complete stabilization of $(2,1)$ tearing modes — even those which have grown to their nonlinear saturation point — can be modeled. We have seen that RF which is injected just outside the rational surface ($R_{rf} = 2.053$ in Figure 6) preemptively renders the plasma equilibrium stable to tearing modes at RF input powers $> 1\%$. Application of the same RF parameters in the presence of saturated tearing modes, therefore, ought to yield stability as the transient behaviors associated with the Δ'_{ECCD} term of Eq. (26) decay in time, and this is confirmed in Figures 7 and 8 (for which the current ratio $I_{RF}/I_0 \approx 3\%$). In Figure 7, various low–order Fourier components of the volume–integrated magnetic energy are plotted as the discharge evolves. Initial linear and Rutherford–type growth of the $(2,1)$ magnetic islands raises the $n = 1$ magnetic energy to a saturated state at approximately $t = 0.09$ seconds. Subsequently, as the ECCD amplitude begins to rise, the value of the magnetic energy (which can loosely

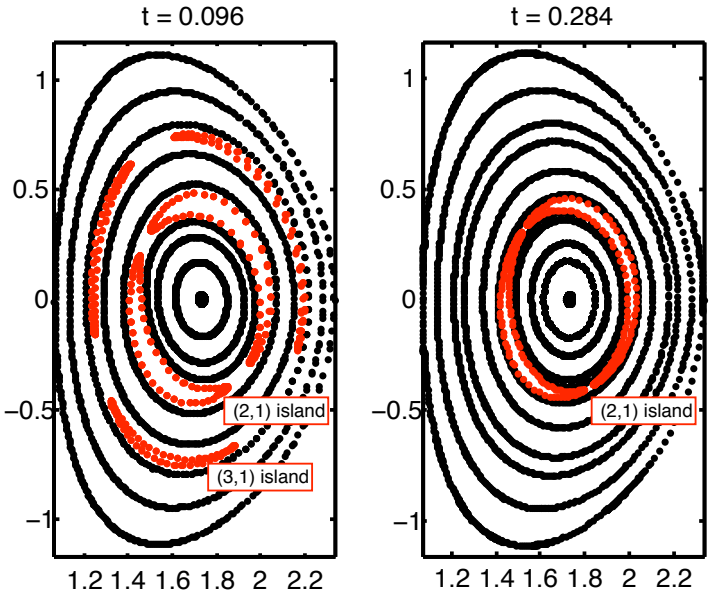

Figure 8: Island structure at various points in the discharge of Figure 7. The saturated state of $(2,1)$ and $(3,1)$ magnetic islands, before ECCD is applied, is shown on the left plot. Roughly three resistive times elapse between this plot and the plot on the right; the vanishing of the $(3,1)$ islands and the reduced widths of $(2,1)$ islands can be seen as the plots are compared. Ultimately, the islands vanish altogether due to the RF.

be associated with $E_{mag} \sim w^4$ where w is the island width) begins to decay at a consistently increasing rate. Explicit plots of the saturated $(2,1)$ island structure ($\sim$ 13 cm wide) are given in Figure 8a, which also reveals the presence of less prominent $(3,1)$ islands (the equilibrium is also weakly unstable to this mode). Figure 8b, obtained at roughly three resistive times after its counterpart, shows that the width of the $(2,1)$ island is reduced in response to the RF and that the $(3,1)$ island has completely vanished. By $t = 0.35$ s, Poincaré plots similar to those of Figure 8 reveal no island structures at all.

The shift in the position of the rational surface in response to RF injection also has important effects on the stabilization or destabilization of the tearing mode. The growth rates corresponding to deposition peaked at $r_{rf} = 1.979$ in Figure 6, for example, initially are highly destabilized by low–amplitude RF injection, but increasing the RF amplitude (and thus the current ratio) appears to have little effect for current ratios above 2%. Figure 9 demonstrates the reason for this effect; the RF steepens the μ profile just inside the rational surface (leading to instability), but as the RF power is increased, the position of the

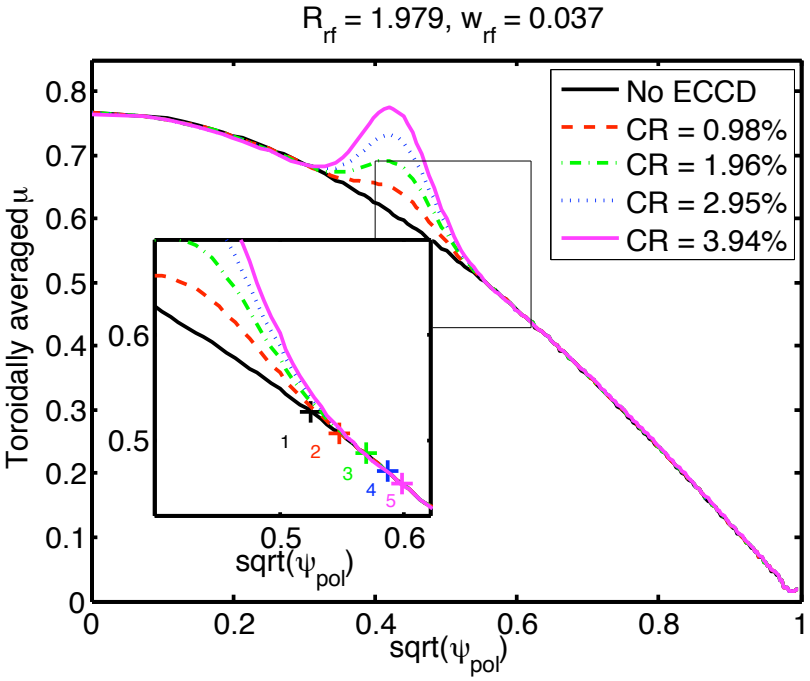

Figure 9: Toroidally averaged μ profile of the plasma in response to RF perturbations of increasing current ratio CR $\equiv I_{RF}/I_0$ (as in Figures 5 – 6) centered at $R_{rf} = 1.979$ m. (Inset) Crosses denote the $(2,1)$ rational surface position for each profile (increasing numbers correspond to increasing current ratios). Although the RF perturbations initially steepen this profile near the rational surface (a destabilizing effect), the rational surface position shifts radially outward as the RF power is increased. Thus, the steepening cannot persist, and further increasing the current ratio (as the "o" markers of Figure 6 indicate) has relatively little influence on the growth rate.

rational surface is shifted outward away from the profile modifications. A more meaningful consequence of this phenomena can be seen in Figure 10, wherein the long–time effects of RF drive peaked just outside the rational surface ($r_{rf} = 2.053$) stabilize the mode completely at high input powers. Here, the μ profile flattens at the rational surface; its slope becomes less and less negative, even becoming positive for high current ratios. However, as the RF power/current ratio is increased, the position of the rational surface again shifts outward. At higher RF powers, as it crosses the peak of the RF–induced perturbation of μ, its slope will again become negative, and instability will result. This effect is also present in Figure 6 of Pletzer and Perkins (the black diamonds in their plot); the destabilizing effect of RF deposition centered on the rational surface and applied at increasingly high powers arises from the associated outward shift of the rational surface.

We surmise from these results that Δ' stabilization of the resistive tearing modes in this model is highly sensitive to the location of the ECCD deposition (as is also the case in experimental efforts to suppress their neoclassical counterparts). In a sense, one is attempting to hit a moving target; the Δ'–stabilizing effect of RF is maximized by highly localized deposition just outside the mode rational surface, but the surface itself also moves in response to the RF perturbation. Nevertheless, we have demonstrated that complete stabilization of the mode is possible, provided that the RF is applied at the appropriate place and that sufficient time has elapsed for the flux–surface averaged parallel currents to be the dominant term in the parallel Ohm's law. We now consider the effects of the ECCD at short times, when the latter assumption is invalid.

4 Effects of ECCD deposition on resistive tearing modes — the short–time limit

In addition to the long–time effects of Δ' stabilization discussed in the previous sections, the short–time effects of the Δ'_{ECCD} term in Eq. (26) can influence the growth of resistive tearing modes. The helical current fluctuations induced by RF deposition at short times, which are associated with Alfvén wave propagation on the plasma flux surfaces, compete with the helical currents associated with the mode itself as it grows, and can either counteract or reinforce these currents depending on their orientation relative to the magnetic island.

In experiments, the use of ECCD to suppress or mitigate the effects of tearing modes can proceed either preemptively (wherein plasma profiles anticipated to exhibit tearing instabilities are tailored by the use of RF so that these instabilities do not arise) or reactively (wherein the detection of island structures within the plasma triggers the application of RF to appropriately counter them). The former technique is more closely associated with the Δ' stabilization of the previous section; we are applying RF to an unstable profile in an effort to alter the profile before the instability arises. The latter (reactive) technique, however, is more closely tied to Δ'_{ECCD} stabilization, as it is desirable to counter

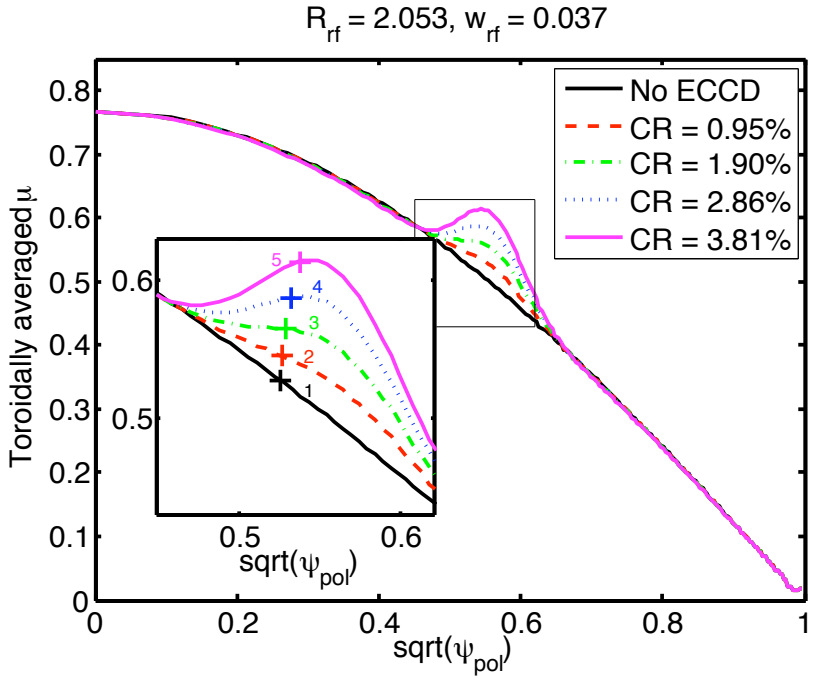

Figure 10: Toroidally averaged μ profile of the plasma in response to RF perturbations of increasing current ratio centered at $R_{rf} = 2.053$ m. (Inset) The $(2, 1)$ rational surface positions are again marked with crosses. RF perturbations initially flatten the profile near the rational surface, yielding a net stabilizing effect. As the current ratio increases, however, the position of the rational surface moves outward in $\sqrt{\psi_{pol}}$ toward the RF–induced peak in $\langle\mu\rangle$. Instability will result if the RF power is sufficiently large, due to the change in profile shape as the peak is crossed.

the growth of existing islands on a short, rather than long, timescale. As a means of illustrating the differing physics associated with these processes, we repeat the procedure of the previous section and initially evolve only toroidally symmetric components of the MHD equations. However, we allow the growth of the tearing mode after only short times have passed. The induced, flux–surface averaged parallel current which alters Δ' rises to 99% of its peak value very slowly in these cases — roughly twenty resistive times elapse before the Δ' modification has neared its peak value [agreeing qualitatively with Eq. (23) in that the rise time for the current is a resistive time multiplied by a constant (geometric) factor]. Thus, if the tearing mode is allowed to grow after only one or two resistive times have passed, we may expect that the dominant effects on the mode growth will arise from the Δ'_{ECCD} term of Eq. (26).

I_{RF}/I_0	R_{rf}	γ_1	γ_2	γ_{20}
0.0000	—	371.88	371.88	371.88
0.0100	1.942	683.89	660.31	518.49
0.0200	1.942	888.35	781.23	539.39
0.0300	1.942	1021.72	800.50	480.94
0.0400	1.942	1135.77	799.41	397.78
0.0098	1.979	1100.91	1094.48	834.50
0.0196	1.979	1754.99	1659.61	1039.10
0.0295	1.979	2334.12	2061.38	1113.18
0.0394	1.979	2868.37	2350.39	1088.91
0.0097	2.016	390.29	465.04	543.45
0.0193	2.016	809.85	1089.22	1197.43
0.0290	2.016	1689.10	2207.50	1854.23
0.0387	2.016	2919.87	3516.81	2250.62
0.0095	2.053	104.18	86.03	13.39
0.0190	2.053	29.32	0.00	0.00
0.0286	2.053	187.45	79.15	0.00
0.0381	2.053	522.13	524.81	0.00
0.0094	2.090	453.34	448.92	389.69
0.0187	2.090	494.42	485.79	417.78
0.0281	2.090	546.98	515.96	452.30
0.0374	2.090	593.47	560.39	509.67

Table 1: Growth rates of the $(2,1)$ tearing mode in response to RF deposition of various powers and locations on the outboard midplane. The RF rise time t_p [see Eq. (29)] is 0.064, which is equal to the resistive time τ_R; the growth rate γ_1 is calculated when the RF attains 99% of its maximum value. After an additional τ_R has elapsed, γ_2 is calculated; the growth rate in the long–time limit (corresponding to Δ' modification of the equilibrium profile) is given by γ_{20} (approximately 20 resistive times are required to drive the flux–surface averaged toroidal current up to 99% of its maximum value).

Table 1 demonstrates the effect of the Δ'_{ECCD} term in Eq. (26) on the growth rate of the tearing mode in the simulations which have been discussed so far; the results bear some similarity to the long–time Δ' modifications discussed previously. Deposition markedly outside the mode rational surface ($R_{rf} = 2.090$), as in the long–time limit, appears to elevate the tearing mode growth rates slightly at short times, though the change is relatively small. However, for $R_{rf} = 2.053$, wherein the long–time Δ' modifications yield stability or extremely slow growth, low–power RF injection reduces the growth rate but does not stabilize the mode at short times. In addition, RF amplitudes inducing current ratios $> 3\%$ (which are stabilizing in the long–time limit) initially act to *destabilize* the mode at short times. The destabilizing effect is (again) a consequence of the rational surface shift in response to the RF, as was noted in Figure 10. It occurs at lower input powers here because the rational surface does not attain its shifted

value immediately; rather, it moves through regions of the profile which may promote stability or instability as it approaches its final state.

In general, deposition just inside the rational surface is destabilizing both at long and short times; in the latter case the destabilization may be quite extreme (approaching an order of magnitude increase in the growth rate, in a number of cases). In such cases, the short–time behavior of the mode indicates that radial alignment of the RF deposition will also be detrimental in the long–time limit. Short–time reductions of the mode growth rate in response to low RF input powers, however, can serve as a signature of proper alignment leading to eventual long–time stability.

5 Summary and conclusions

In this work, we have demonstrated that a viable model describing the interaction of RF (in the form of ECCD) with MHD can be constructed. We have also shown that relevant details of the physics of localized ECCD deposition are captured by this model despite its lack of full self–consistency (in that local heating effects and the effects of RF in the MHD closure are neglected). Localized current drive induces Alfvénic disturbances along magnetic field lines, resulting in helical and spatially fluctuating current filaments at short times and a net flux–surface averaged current on longer timescales. This average current is responsible for modifications of the matching index Δ', while the helical filaments arising at short times interfere with or enhance the helical currents associated with the tearing mode structure to influence the growth. Favorable comparisons with the results of Pletzer and Perkins [24] have been demonstrated; the optimal position for RF deposition is verified to be immediately outside the initial rational surface on which the mode grows, and the destabilizing effects induced by the shift of this surface in response to RF perturbations (which also arise in the former work) are correctly produced.

We believe that this work is an important step forward in the development of integrated, predictive models for ECCD/MHD interactions (such as, for example, might be used to determine optimum NTM stabilization approaches in ITER). Our model utilized toroidally symmetric ECCD deposition, with the poloidal localization of the RF fields being given essentially as an *ad hoc* function. The former assumption, though clearly not appropriate in all cases, has been used successfully to explain experimental observations [21] and is a useful approximation for plasmas undergoing rapid toroidal rotation. A more realistic model (which is a topic of ongoing research) could utilize data from ray tracing codes to determine the amplitude and spatial localization of the ECCD–induced electromotive forces. NIMROD's magnetic geometry, for instance, can be exported to the GENRAY/CQL3D [39] code, which can then calculate ray trajectories and power deposition associated with a particular ECCD configuration. The physics of these coupled simulations can then be cross–checked against the conclusions of this work for consistency, and effects arising from the development of accurate closure models (which account for the effects of RF

on the higher–order velocity moments) can also be compared with these results to determine the additional physics imparted by the closures. These developments, along with the rigorous verification of self–consistency among collision operators, quasilinear operators, and fluid equations, will serve as future steps of importance in the development of an integrated ECCD/MHD model.

6 Acknowledgements

This work is supported by the SciDAC Center for Simulation of RF Wave Interactions with Magnetohydrodynamics (SWIM) and by the U. S. Department of Energy. We wish to thank F. Ebrahimi, J. Carlsson, E. D. Held, J.-Y. Ji, J. D. Callen, R. W. Harvey, A. P. Smirnov, and D. B. Batchelor, as well as members of the NIMROD team and the SciDAC Center for Extended MHD Modeling (CEMM), for useful discussion and feedback.

A The coupled RF/MHD equations

In this section, we discuss the sense in which Eqs. (1 - 7) accurately approximate the fully self–consistent interaction of RF ECCD injection with MHD. Because detailed treatments of the derivation of MHD equations can be found elsewhere (e.g., [40]), we provide only a brief sketch of how the derivation is modified in the presence of RF.

The starting point for the derivation of MHD equations is a kinetic equation for the distribution function $\tilde{f}_\alpha = \tilde{f}_\alpha(\mathbf{x}, \mathbf{v}, t)$ of species α;

$$\frac{\partial \tilde{f}_\alpha}{\partial t} + \mathbf{v} \cdot \nabla \tilde{f}_\alpha + \frac{q_\alpha}{m_\alpha} \left[\tilde{\mathbf{E}}(\mathbf{x}, t) + \mathbf{v} \times \tilde{\mathbf{B}}(\mathbf{x}, t) \right] \cdot \frac{\partial \tilde{f}_\alpha}{\partial \mathbf{v}} = C(\tilde{f}_\alpha) \ , \qquad (30)$$

wherein the electric and magnetic fields $\tilde{\mathbf{E}}(\mathbf{x}, t)$ and $\tilde{\mathbf{B}}(\mathbf{x}, t)$ are determined by Maxwell's equations (containing charge and current densities from these distribution functions as source terms). When localized ECCD is applied, both the distribution function and the fields can vary on the rapid timescales associated with the propagation of RF waves through the plasma. (We place a tilde over quantities which may vary on this timescale). The dynamics of interest, however, concern the slower, self–consistent interaction of fields and distribution functions which give rise to two–fluid and MHD phenomena. To proceed, one may average over a few wave periods of the rapid timescale (denoted $\langle \cdot \rangle_t$) and make a quasilinear approximation [41, 42] for the ECCD effects. Heuristically, the kinetic equation for the short–time–averaged distribution function $f_\alpha \equiv \langle \tilde{f}_\alpha \rangle_t$ then takes the form

$$\frac{\partial f_\alpha}{\partial t} + \mathbf{v} \cdot \nabla f_\alpha + \frac{q_\alpha}{m_\alpha} \left[\mathbf{E}(\mathbf{x}, t) + \mathbf{v} \times \mathbf{B}(\mathbf{x}, t) \right] \cdot \frac{\partial f_\alpha}{\partial \mathbf{v}} = C(f_\alpha) + Q(f_\alpha) \ , \qquad (31)$$

wherein the ECCD/MHD interaction is represented by the $Q(f_e)$ operator. The ions are presumed to be unaffected by the RF, i.e. $Q(f_i) = 0$, and one observes

that the rapid time variation has also been removed from the electromagnetic fields. As velocity moments of the kinetic equation are taken to obtain the fluid/MHD equations, we obtain velocity–space integrals over $Q(f_e)$.

A.1 Zeroth velocity moment

The direct integration of Eq. (31) over the velocity space yields a continuity equation for the ion and electron fluids. Since ECCD ordinarily neither creates nor destroys particles in fusion plasmas, the velocity–space integral of $Q(f_e)$ must be zero; both the two–fluid and MHD continuity equations [see Eq. (4)] are unaffected by the RF.

A.2 First velocity moment

The product of $m_\alpha \mathbf{v}$ and the kinetic equation (31), when integrated over the velocity space, yields momentum equations for the ion and electron fluids,

$$m_\alpha n_\alpha \frac{\partial \mathbf{u}_\alpha}{\partial t} + m_\alpha n_\alpha (\mathbf{u}_\alpha \cdot \nabla)\mathbf{u}_\alpha = -\nabla p_\alpha - \nabla \cdot \overleftrightarrow{\mathbf{\Pi}}_\alpha + n_\alpha q_\alpha [\mathbf{E} + \mathbf{u}_\alpha \times \mathbf{B}] + \mathbf{R}_\alpha + \mathbf{F}_\alpha^{rf} \tag{32}$$

wherein the subscripted quantities $n, \mathbf{u}, p, \Pi, \mathbf{R}$, and $\mathbf{F}^{rf}$ are respectively the density, velocity, scalar pressure, anisotropic pressure tensor, and momentum transfer due to collisional friction/RF injection for species α. Summing Eq. (32) over species yields an MHD momentum equation which is similar to Eq. (5), but which contains an additional term representing the transfer of momentum from RF waves to electrons. Because of the large mass ratio, this additional term is small enough relative to the ion momentum that its neglect is justifiable. However, the corresponding term cannot be dropped in the MHD Ohm's law [obtained from the electron version of Eq. (32)] because it may be of the same order as the plasma's (small) electric field. Assuming that a small–ion–gyroradius approximation can be used to drop diamagnetic and Hall terms, the Ohm's law takes the form

$$\mathbf{E} + \mathbf{u} \times \mathbf{B} = \eta \mathbf{J} + \frac{\mathbf{F}_e^{rf}}{n|q_e|} \tag{33}$$

where the final term on the right–hand side incorporates the RF effects. The $\mathbf{F}_e^{rf}$ term has the explicit form

$$\mathbf{F}_e^{rf} = \int m_e (\mathbf{v} - \mathbf{u}_e) Q(f_e) d^3\mathbf{v} \ , \tag{34}$$

and captures the dominant physics of the ECCD/MHD interaction.

A.3 Second velocity moment

Integration of the product of $m_\alpha(\mathbf{v} - \mathbf{u}_\alpha) \cdot (\mathbf{v} - \mathbf{u}_\alpha)/2$ with the kinetic equation (31) yields an equation for the temperature T_α of a given species;

$$\frac{3}{2}n_\alpha\frac{\partial T_\alpha}{\partial t}+\frac{3}{2}n_\alpha(\mathbf{u}_\alpha\cdot\nabla)T_\alpha+n_\alpha T_\alpha\nabla\cdot\mathbf{u}_\alpha=-\nabla\cdot\mathbf{q}_\alpha-\overleftrightarrow{\mathbf{\Pi}}_\alpha\colon[\nabla\mathbf{u}_\alpha]+Q_\alpha+S^{rf}_\alpha\ , \quad (35)$$

wherein the subscripted quantities $\mathbf{q}, Q$, and S^{rf} represent the heat flux, collisional heating, and RF heating experienced by fluids of species α. Summing this equation over species and dropping small terms (which relate to the small difference between ion and electron velocities) yields the standard MHD equation (7) describing the evolution of plasma temperature, as well as a new term representing the effects of localized electron heating imparted by the ECCD. As was the case in the momentum equation, however, the net influence of this heating can be neglected in light of the mass ratio and the generally small effect of collisional ion heating (to which ECCD–induced heating may be compared) to the plasma temperature evolution.

A.4 Closures

In addition to the complexities of the standard MHD closure problem [32], the calculation of a physically consistent closure for our coupled ECCD/MHD model must take into account the presence of the quasilinear RF operator $Q(f_e)$ in the kinetic equation. In general, the closure problem entails the determination of values for heat fluxes ($\mathbf{q}$) and stresses ($\mathbf{\Pi}$) as functions of lower–order fluid moments. In this work, the effects of the quasilinear operator on the closure are not considered; rather, we utilize the approximate Braginskii closures of the NIMROD code to determine $\mathbf{q}$ and $\mathbf{\Pi}$. Specifically, we have

$$\mathbf{\Pi} \equiv -\rho\nu\nabla\mathbf{u} \quad (36)$$

$$\mathbf{q} \equiv \frac{3n}{2}\chi\cdot\nabla T \quad (37)$$

$$\chi \equiv \kappa_\parallel\hat{b}\hat{b}+\kappa_\perp(\mathbf{I}-\hat{b}\hat{b}) \quad (38)$$

wherein n is the number density, $\mathbf{I}$ is the unit tensor, and $\hat{b}$ is the direction of the local magnetic field. The numerical parameters $\nu, \kappa_\parallel$, and $\kappa_\perp (\ll \kappa_\parallel)$ represent kinetic viscosity and parallel/perpendicular heat diffusivity; in this work, typical values for these parameters are respectively $4.3\times10^{-2}, 4.3\times10^{7}$, and 4.3×10^{1}.

A.5 Summary

As demonstrated above, the most significant alteration to the conventional system of resistive MHD equations by localized ECCD deposition is the additional term on the right–hand side of Ohm's law, Eq. (33). From the single–fluid MHD perspective, one may associate this term with an electromotive force density induced by the RF waves on the fluid, and a meaningful approximation to the fully self–consistent ECCD/MHD problem is thus obtained by determining the response of the resistive MHD system to this emf. Our approach in this

work, therefore, has been to (a) specify a form for this term which is reasonably consistent with ECCD deposition profiles in experiments, (b) determine the response of tearing modes arising in the model ECCD/MHD system to various RF inputs, and (c) check the consistency of the system against known results. In doing so, we gain insight into the physical processes which will arise in more comprehensive simulation models.

References

[1] C. C. Hegna, Phys. Plasmas **5**, 1767 (1998).

[2] R. J. La Haye, Phys. Plasmas **13**, 055501 (2006).

[3] H. Zohm, A. Kallenbach, H. Bruhns, G. Fussmann, and O. Klüber, Europhys. Lett. **11**, 745 (1990).

[4] Z. Chang, E. D. Fredrickson, J. D. Callen, K. M. McGuire, M. G. Bell, R. V. Budny, C. E. Bush, D. S. Darrow, A. C. Janos, L. C. Johnson, H. K. Park, S. D. Scott, J. D. Strachan, E. J. Synakowski, G. Taylor, R. M. Wieland, M. C. Zarnstorff, S. J. Zweben, and the TFTR Group, Nucl. Fusion **34**, 1309 (1994).

[5] S. Günter, A. Gude, M. Maraschek, and Q. Yu, , Plasma Phys. Controlled Fusion **41**, 767 (1999).

[6] E. J. Strait, L. Lao, A. G. Kellman, T. H. Osborne, R. Snider, R. D. Stambaugh, and T. S. Taylor, Phys. Rev. Lett. **62**, 1282 (1989).

[7] O. Sauter, R. J. La Haye, Z. Chang, D. A. Gates, Y. Kamada, H. Zohm, A. Bondeson, D. Boucher, J. D. Callen, M. S. Chu, T. A. Gianakon, O. Gruber, R. W. Harvey, C. C. Hegna, L. L. Lao, D. A. Monticello, F. Perkins, A. Pletzer, A. H. Reiman, M. Rosenbluth, E. J. Strait, T. S. Taylor, A. D. Turnbull, F. Waelbroeck, J. C. Wesley, H. R. Wilson, and R. Yoshino, Phys. Plasmas **4**, 1654 (1997).

[8] R. J. La Haye, L. L. Lao, E. J. Strait, and T. S. Taylor, Nucl. Fusion **37**, 397 (1997).

[9] R. J. La Haye, B. W. Rice, and E. J. Strait, Nucl. Fusion **40**, 53 (2000).

[10] A. Isayama, Y. Kamada, N. Hayashi, T. Suzuki, T. Oikawa, T. Fujita, T. Fukuda, S. Ide, H. Takenaga, K. Ushigusa, T. Ozeki, Y. Ikeda, N. Umeda, H. Yamada, M. Isobe, Y. Narushima, K. Ikeda, S. Sakakibara, K. Yamazaki, K. Nagasaki and the JT–60 Team, Nucl. Fusion **43**, 1272 (2003).

[11] Q. Yu, S. Günter, K. Lackner, A. Gude, and M. Maraschek, Nucl. Fusion **40**, 2031 (2000).

[12] R. J. La Haye, S. Günter, D. A. Humphreys, J. Lohr, T. C. Luce, M. E. Maraschek, C. C. Petty, R. Prater, J. T. Scoville, and E. J. Strait, Phys. Plasmas **9**, 2051 (2002).

[13] N. J. Fisch, Rev. Mod. Phys. **59**, 175 (1987).

[14] C. C. Hegna and J. D. Callen, Phys. Plasmas **4**, 2940 (1997).

[15] H. Zohm, Phys. Plasmas **4**, 3433 (1997).

[16] H. Zohm, G. Gantenbein, A. Gude, S. Günter, F. Leuterer, M. Maraschek, J. P. Meskat, W. Suttrop, Q. Yu, ASDEX Upgrade Team, and ECRH Group (AUG), Nucl. Fusion **41**, 197 (2001).

[17] H. Zohm, G. Gantenbein, G. Giruzzi, S. Günter, F. Leuterer, M. Maraschek, J. Meskat, A. G. Peeters, W. Suttorp, D. Wagner, M. Zabiégo, ASDEX Upgrade Team, and ECRH Group, Nucl. Fusion **39**, 577 (1999).

[18] G. Gantenbein, H. Zohm, G. Giruzzi, S. Günter, F. Leuterer, M. Maraschek, J. Meskat, Q. Yu, ASDEX Upgrade Team, and ECRH–Group (AUG), Phys. Rev. Lett. **85**, 1242 (2000).

[19] A. Isayama, Y. Kamada, T. Ozeki, S. Ide, T. Fujita, T. Oikawa, T. Suzuki, Y. Neyatani, N. Isei, K. Hamamatsu, Y. Ikeda, K. Takahashi, K. Kajiwara, and the JT–60 Team, Nucl. Fusion **41**, 761 (2001).

[20] C. C. Petty, R. J. La Haye, T. C. Luce, D. A. Humphreys, A. W. Hyatt, J. Lohr, R. Prater, E. J. Strait, and M. R. Wade, Nucl. Fusion **44**, 243 (2004).

[21] R. J. La Haye, J. R. Ferron, D. A. Humphreys, T. C. Luce, C. C. Petty, R. Prater, E. J. Strait, and A. S. Welander, Nucl. Fusion **48**, 054004 (2008).

[22] R. Prater, R. J. La Haye, J. Lohr, T. C. Luce, C. C. Petty, J. R. Ferron, D. A. Humphreys, E. J. Strait, F. W. Perkins, and R. W. Harvey, Nucl. Fusion **43**, 1128 (2003).

[23] D. A. Humphreys, J. R. Ferron, R. J. La Haye, T. C. Luce, C. C. Petty, R. Prater, and A. S. Welander, Phys. Plasmas **13**, 056113 (2006).

[24] A. Pletzer and F. W. Perkins, Phys. Plasmas **6**, 1589 (1999).

[25] N. Hayashi, T. Ozeki, K. Hamamatsu, and T. Takizuka, Nucl. Fusion **44**, 477 (2004).

[26] R. J. La Haye, R. Prater, R. J. Buttery, N. Hayashi, A. Isayama, M. E. Maraschek, L. Urso, and H. Zohm, Nucl. Fusion **46**, 451 (2006).

[27] The SciDAC Center for Simulation of RF Wave Interactions with Magnetohydrodynamics (SWIM), which funds this work, attempts to address various forms of the general RF/MHD interaction problem through the self–consistent coupling of disparate physics codes. See http://cswim.org for further details.

[28] G. Giruzzi, M. Zabiégo, T. A. Gianakon, X. Garbet, A. Cardinali, S. Bernabei, Nucl. Fusion **39**, 107 (1999).

[29] G. D. Kerbel and M. G. McCoy, Phys. Fluids **28**, 3629 (1985).

[30] M. Sharma, E. D. Held, and J.-Y. Ji, Bull. APS **53** (abstract only), 39 (2008).

[31] C. C. Hegna and J. D. Callen, to be published (2009).

[32] J.-Y. Ji and E. D. Held, Phys. Plasmas **13**, 102013 (2006).

[33] J. J. Ramos, Phys. Plasmas **15**, 082106 (2008).

[34] C. R. Sovinec, A. H. Glasser, T. A. Gianakon, D. C. Barnes, R. A. Nebel, S. E. Kruger, D. D. Schnack, S. J. Plimpton, A. Tarditi, M. S. Chu, and the NIMROD Team, J. Comp. Phys. **195**, 355 (2004).

[35] Information and documentation for NIMROD is available at http://nimrodteam.org.

[36] P. H. Rutherford, Phys. Fluids **16**, 1903 (1973).

[37] O. Sauter, Phys. Plasmas **11**, 4808 (2004).

[38] R. B. White, Rev. Mod. Phys. **58**, 183 (1986).

[39] Information and documentation for GENRAY/CQL3D is available at http://www.compxco.com.

[40] J. P. Freidberg, Rev. Mod. Phys. **54**, 801 (1982).

[41] C. F. Kennel and F. Engelmann, Phys. Fluids **9**, 2377 (1966).

[42] A. N. Kaufman, Phys. Fluids **15**, 1063 (1972).

UW-Madison SWIM Slow MHD Campaign - FY 2009 Report

Notable accomplishments

- NIMROD and GENRAY can now export their data structures to one another, enabling GENRAY to calculate ray trajectories in NIMROD equilibria and NIMROD to calculate local ECCD deposition from GENRAY ray data. Robust methods for processing of ray data (calculation of relevant volume elements; interpolation of discrete ray data onto NIMROD's finite elements) have been developed and tested.
- NIMROD interfacing with the Integrated Plasma Simulator framework is well under way. Component script logic for coupled NIMROD/GENRAY simulation has been developed; at present, these scripts run NIMROD's preprocessing utilities and interface GENRAY to the plasma state. Coupled, IPS-driven simulations are anticipated imminently as work on the NIMROD interface proceeds.
- Quantitative agreement with the tearing mode stabilization work of Pletzer/Perkins [Phys. Plasmas 6, 1589 (1999)] has been obtained; as well, the role of rational surface motion in response to ECCD deposition has been shown to account for previously unexplored destabilizing effects (presented in that work) induced by large ECCD amplitudes at the unperturbed rational surface position.
- Initial studies of MHD response to RF deposition models have shown good agreement with Hegna/Callen [Phys. Plasmas 4, 2940 (1997)] predictions for island size/response and with ECCD alignment studies of La Haye et al. [Nucl. Fusion 48, 054004 (2008)]. Complete suppression of the resistive tearing mode by adequately aligned ECCD of sufficient amplitude has been demonstrated by a model case.

Publications

- T. Jenkins et al., "Calculating electron cyclotron current drive stabilization of resistive tearing modes in a nonlinear MHD model", in review at Phys. Plasmas.
- C. C. Hegna and J. D. Callen, "A closure scheme for modeling rf modifications to the fluid equations", accepted by Phys. Plasmas.

Conference Presentations

- T. Jenkins et al., "Modeling of RF/MHD coupling using NIMROD and GENRAY", APS-DPP, Dallas, Texas, November 2008. Also presented at NIMROD team meeting and CEMM meeting, Dallas, TX, November 2008.
- T. Jenkins et al., "Modeling of RF/MHD coupling using NIMROD, GENRAY, and the Integrated Plasma Simulator", APS April Meeting/Sherwood Fusion Theory Conference, Denver, CO, May 2009.
- T. Jenkins et al., "Modeling ECCD stabilization of resistive tearing modes", NIMROD team meeting, Denver, CO, May 2009. Also presented at CEMM meeting, Denver, CO, May 2009.
- T. Jenkins, "ECCD-induced resistive tearing mode stabilization and rational surface motion", NIMROD team meeting, Madison, WI, July 2009.

Final Report

for the subcontract from the University of Wisconsin-Madison to Tech-X
for work on
Center for Simulation of Wave Interactions with Magnetohydrodynamics (SWIM)

Thomas G. Jenkins

Abstract

The work conducted by Tech-X Corporation employees via subcontract #7213-001 from the University of Wisconsin-Madison, in furtherance of the research goals outlined in the Center for Simulation of Wave Interactions with Magnetohydrodynamics proposal (U.S. DoE Office of Science Award Number DE-FC02-06ER54899), is summarized. The research is shown to adequately address the research goals in the proposal and Statement of Work, in conjunction with ongoing research funded by SWIM via direct contract with Tech-X Corporation.

1 Overview of the SWIM project

The Center for Simulation of Wave Interactions with Magnetohydrodynamics (SWIM) was begun in 2005 with two major scientific objectives:

- To improve understanding of interactions that both RF wave and particle sources have on extended MHD phenomena, and substantially improve capability for predicting and optimizing the performance of burning plasmas,
- To develop an integrated computational system for treating multi-physics phenomena with the required flexibility and extensibility to serve as a prototype for the Fusion Simulation Project, address the mathematics issues related to the multi-scale, coupled physics of RF waves and extended MHD, and optimize the integrated system on high performance computers.

In furtherance of these goals, project efforts have been directed along three major lines of research:

- **IPS development campaign** — Development of the Integrated Plasma Simulator, a computational platform that allows efficient coupling of a broad range of fusion codes, is flexible enough to allow exploration of various physics models and solution algorithms, that permits convenient user access and access to experimental data, and that is robust to evolving physics, code development, and developments in computer hardware. The IPS contains components to calculate wave propagation and absorption in all relevant frequency regimes, to calculate the modification of the plasma velocity distribution from sources (RF, neutral injection and particles), and to calculate profile and magnetic evolution (assuming closed flux surfaces), as well as linear MHD stability models and reduced models of non-linear MHD events.
- **Fast MHD physics campaign** — Research addressing long timescale discharge evolution in the presence of sporadic fast MHD events. The primary physics focus is to allow the development of optimized burning plasma scenarios, via the use of 3D nonlinear extended MHD codes, and to improve understanding of how RF can be employed to achieve long-time MHD stable discharges and control sawtooth events.
- **Slow MHD physics campaign** — Research modeling the direct interaction of RF and extended MHD for slowly growing modes. The primary physics focus is to improve the understanding of how RF waves (primarily ECCD/ECRH) can be employed to control neoclassical tearing modes.

The work discussed in this report centers on the Slow MHD physics campaign, for which initial work was performed at the University of Wisconsin-Madison by the author (Dr. T. Jenkins). In early 2010, Dr. Jenkins left UW-Madison and began working for Tech-X Corporation; work relevant to UW-Madison's portion of the Slow MHD campaign was subsequently subcontracted

to Tech-X beginning in March 2010. Funding for SWIM was subsequently extended by one year; since Tech-X was already receiving funding directly from SWIM, funds for this final year were reallocated directly to Tech-X (rather than going through UW-Madison). Hence, this report is unusual in that the funding period covers neither the beginning (conducted at UW-Madison from 2007-2009) nor the end of the research effort (to be conducted at Tech-X in 2011 and early 2012), and its designation as a "Final Report" should be construed only to mean that it provides a detailed summary of the current status of SWIM research at the conclusion of the UW-Madison subcontract. The work summarized herein was conducted by Dr. Jenkins, except as noted.

For background, we now summarize the initial work on the SWIM project which was performed at UW-Madison (prior to the beginning of the Tech-X subcontract). In addition to becoming familiar with NIMROD (a 3D nonlinear extended MHD code) and GENRAY (a ray tracing code that calculates propagation trajectories and power deposition of RF waves in a plasma), Dr. Jenkins conducted work in which *ad hoc* RF sources (designed to approximately mimic source terms one would obtain from a self-consistent RF/MHD model) were added to NIMROD. These simulations primarily used toroidally symmetric RF sources. Although this simplifying approximation is primarily applicable to plasmas with very high toroidal rotation velocities, it provides a reasonably simple model in which the various timescales of the RF/MHD stabilization problem can be compared. The effects of these RF sources on resistive tearing modes were investigated and a paper was published [T. G. Jenkins *et al.*, "Calculating electron cyclotron current drive stabilization of resistive tearing modes in a nonlinear MHD model", Phys. Plasmas **17**, 012502 (2010)] summarizing key findings. Key results from this paper include the following:

1. NIMROD's ability to simulate the axisymmetric evolution of the plasma toward an RF-modified steady-state is consistent with the results of Pletzer and Perkins [A. Pletzer and F. W. Perkins, Phys. Plasmas **6**, 1589 (1999)], and the Δ' destabilization observed in the latter work is shown to arise as a consequence of RF-induced rational surface motion.

2. The complete suppression of nonlinearly saturated islands by appropriately aimed RF sources is possible, with this suppression occurring on the inductive timescale (the timescale on which the RF induces plasma current and creates a new, toroidally symmetric steady-state).

3. The short- and long-time responses of the mode rational surface to nearby RF perturbations were investigated, and short-time indicators of favorable RF alignment for toroidally localized sources were specified.

In addition to the aforementioned computational work, theoretical calculations detailing how the RF physics (in the form of quasilinear diffusion coefficients) enters the MHD equations were begun. As well, initial work began on the development of IPS component scripts (designed to transfer data between GENRAY and NIMROD) for the coupled simulations.

2 Research objectives from the Statement of Work

Research objectives from the Statement of Work, compiled at the beginning of the Tech-X subcontract, are listed in this section, together with commentary on how these objectives have been fulfilled or will be fulfilled.

1. Year 1

   (a) *Finish the coupling of NIMROD to the IPS framework (developed by the SWIM Project's CS team).*

   This task was successfully completed. It involved two major efforts - coupling NIMROD to the Plasma State (a datastructure accessible by all codes which use the IPS framework, through which data common to the coupled codes can be accessed) and the creation of an IPS component script that could run NIMROD under IPS control.

   For the Plasma State interface, new subroutines were written in NIMROD to define relevant Plasma State variables, various coordinate transformations were carried out (as necessary) to transfer NIMROD data into Plasma State-like representations, and the NIMROD build system was modified to detect and link Plasma State libraries appropriately as needed. Additional variables necessary for this particular RF/MHD coupling were also added to the Plasma State.

   For the IPS component script development, a python script was created through which NIMROD, together with its preprocessors and plotting routines, could be run via IPS commands. Simulations were run to verify that this script behaved as expected; in the process, beneficial experience with the setup and execution of IPS simulations was gained.

   (b) *Couple GENRAY's quasilinear operator to NIMROD, using the IPS framework. Develop an analytic model to verify the accuracy of the code coupling.*

   This task was successfully completed, but was very time-consuming. First, the theoretical calculation detailing how the RF physics (in the form of quasilinear diffusion coefficients) enters the MHD equations was completed. The quasilinear operator was shown to have the form

$$Q(f_\alpha) = -\frac{\partial}{\partial \mathbf{v}} \cdot \left\{ \frac{\epsilon^2 q_\alpha}{(2\pi L)^3 m_\alpha} \int [\mathbf{E}^*_{RFm}(\mathbf{k}) + \frac{\mathbf{v} \times [\mathbf{k} \times \mathbf{E}^*_{RFm}(\mathbf{k})]}{[\omega(\mathbf{k}) - i\Gamma(\mathbf{k})]}] f_{\alpha RFm}(\mathbf{k}, \mathbf{v})\ d^3\mathbf{k} \right\} \quad (1)$$

   with

$$f_{\alpha RFm}(\mathbf{k}, v_{\perp m}, v_{\parallel m}, \phi_m) = -iG_{\alpha m}[\mathbf{E}_{RFm}(\mathbf{k}) \cdot \mathbf{U}_{0\alpha}]$$

$$+\sum_{p=-\infty}^{\infty}\sum_{n=-\infty}^{\infty}\left\{J_n\left(z_{\alpha m}\right)E_{\parallel m}v_{\parallel m}\ +E_m^+v_{\perp m}J_{n-1}\left(z_{\alpha m}\right)\right.$$

$$\left.+E_m^-v_{\perp m}J_{n+1}\left(z_{\alpha m}\right)\right\}\frac{iL_{\alpha m}G_{\alpha m}e^{i(p-n)\phi_m}J_p\left(z_{\alpha m}\right)}{H_{\alpha m}-n\Omega_{\alpha m}} \tag{2}$$

and wherein

$$H_{\alpha m}(\mathbf{k},\mathbf{v})\equiv\left[\omega(\mathbf{k})+i\Gamma(\mathbf{k})-k_{\parallel m}v_{\parallel m}\right] \tag{3}$$

$$z_{\alpha m}(\mathbf{k},\mathbf{v})\equiv\frac{k_{\perp m}v_{\perp m}}{\Omega_{\alpha m}} \tag{4}$$

$$G_{\alpha m}(\mathbf{k},\mathbf{v})\equiv\frac{q_\alpha f_{M\alpha m}(\mathbf{v})}{T_{0\alpha}[\omega(\mathbf{k})+i\Gamma(\mathbf{k})]} \tag{5}$$

$$L_{\alpha m}(\mathbf{k},\mathbf{v})\equiv[\omega(\mathbf{k})+i\Gamma(\mathbf{k})-\mathbf{k}\cdot\mathbf{U}_{0\alpha}] \tag{6}$$

$$f_{M\alpha m}(\mathbf{v})=n_{0\alpha}(\mathbf{x},t)\left(\frac{m_\alpha}{2\pi T_{0\alpha}(\mathbf{x},t)}\right)^{3/2}\cdot$$

$$\exp\left(\frac{-m_\alpha[\mathbf{v}-\mathbf{U}_{0\alpha}(\mathbf{x},t)]\cdot[\mathbf{v}-\mathbf{U}_{0\alpha}(\mathbf{x},t)]}{2T_{0\alpha}(\mathbf{x},t)}\right) \tag{7}$$

The $J_n(z)$ functions are Bessel functions. GENRAY calculates ray trajectories for a particular value of $\mathbf{k}$, yielding a Dirac delta function in the $\mathbf{k}$-integral. Thereafter, the velocity integrals can be carried out to yield modified Bessel functions and (by use of windowed Fourier transforms and the Plemelj formalism) quantities that depend on the wavenumber spectrum of the electric field of the RF waves. The L^{-3} factor in the quasilinear coefficient is related to the various scale lengths of the problem. Because the spatiotemporal scales of the RF physics are considerably smaller than the spatiotemporal scales of MHD phenomena, short-wavelength RF quantities beat together to yield ponderomotive-like quasilinear diffusion on the MHD scales. The volume described by L^{-3} can be thought of as a portion of the collective bundle of rays which GENRAY introduces to the NIMROD plasma; it contains a direction of propagation in one dimension and an area-perpendicular- to-flow in the two orthogonal dimensions. The full quasilinear operator, after integration, contributes terms to the momentum and energy equations of MHD, as well as to Ohm's law. These terms are given by

$$\mathbf{F}_e^{rf}=\frac{\omega_{pe}^2}{\omega}\frac{P}{N_\parallel}\frac{e^{-\xi^2}}{(\mathbf{N}\cdot\sigma)\pi^{5/2}}\left(\frac{\mathbf{N}}{c}\right)\frac{\sqrt{m_e}}{\sqrt{T_e}}\frac{e^{-\lambda}}{2^{3/2}}\cdot$$

$$\left\{|e_\parallel|^2I_n(\lambda)\xi^2+|e_+|^2[\lambda I_n(\lambda)+(n-\lambda)I_{n-1}(\lambda)]\right.$$

$$\left.+|e_-|^2[\lambda I_n(\lambda)-(n+\lambda)I_{n-1}(\lambda)]+\xi(e_\parallel e_+^*+e_\parallel^*e_+)\frac{\sqrt{\lambda}}{\sqrt{2}}[I_{n-1}(\lambda)-I_n(\lambda)]\right.$$

$$+\xi(e_\parallel e_-^* + e_\parallel^* e_-)\frac{\sqrt{\lambda}}{\sqrt{2}}[I_n(\lambda) - I_{n+1}(\lambda)]$$
$$+ (e_+^* e_- + e_-^* e_+)[\lambda I_{n+1}(\lambda) + (n-\lambda)I_n(\lambda)]\big\} \quad (8)$$

$$S_e^{rf} = \frac{\omega_{pe}^2}{\omega c}\frac{P}{N_\parallel}\frac{e^{-\xi^2}}{(\mathbf{N}\cdot\sigma)\pi^{5/2}}\frac{\sqrt{m_e}}{\sqrt{T_e}}\frac{e^{-\lambda}}{2^{3/2}}\cdot$$
$$\big\{|e_\parallel|^2 I_n(\lambda)\xi^2 + |e_+|^2[\lambda I_n(\lambda) + (n-\lambda)I_{n-1}(\lambda)]$$
$$+|e_-|^2[\lambda I_n(\lambda) - (n+\lambda)I_{n-1}(\lambda)] + \xi(e_\parallel e_+^* + e_\parallel^* e_+)\frac{\sqrt{\lambda}}{\sqrt{2}}[I_{n-1}(\lambda) - I_n(\lambda)]$$
$$+\xi(e_\parallel e_-^* + e_\parallel^* e_-)\frac{\sqrt{\lambda}}{\sqrt{2}}[I_n(\lambda) - I_{n+1}(\lambda)]$$
$$+ (e_+^* e_- + e_-^* e_+)[\lambda I_{n+1}(\lambda) + (n-\lambda)I_n(\lambda)]\big\} \quad (9)$$

wherein P is the power content of the RF wave at a particular ray point, σ is the area-perpendicular-to-flow at that point, n is the harmonic number of the cyclotron resonance, I_n is a modified Bessel function, $\mathbf{N} = \mathbf{k}c/\omega$ is the index of refraction, ω is the wave frequency, and

$$\xi = \frac{(\omega - n\Omega_e)}{k_\parallel}\sqrt{\frac{m_e}{2T_e}} \quad (10)$$
$$\lambda = \frac{N_\perp^2 \omega^2 T_e}{c^2 m_e \Omega_e^2} \quad (11)$$
$$e_\parallel = \frac{E_\parallel}{\sqrt{|\mathbf{E}|^2}} \quad (12)$$
$$e_+ = \frac{E_x + iE_y}{\sqrt{|\mathbf{E}|^2}} \quad (13)$$
$$e_- = \frac{E_x - iE_y}{\sqrt{|\mathbf{E}|^2}}\ . \quad (14)$$

All other terms have their conventional meanings. The RF terms enter the MHD equations in the Ohm's Law, momentum, and energy equations (respectively) in the following manner, with conventional notation being used:

$$\mathbf{E} + \mathbf{u}\times\mathbf{B} = \eta\mathbf{J} + \frac{\mathbf{F}_e^{rf}}{n|q_e|} \quad (15)$$
$$\rho\frac{\partial \mathbf{u}}{\partial t} + \rho(\mathbf{u}\cdot\nabla)\mathbf{u} = -\nabla p + \mathbf{J}\times\mathbf{B} - \nabla\cdot\Pi + \mathbf{F}_e^{rf} \quad (16)$$
$$\frac{3}{2}n\left(\frac{\partial T}{\partial t} + (\mathbf{u}\cdot\nabla)T\right) + p\nabla\cdot\mathbf{u} = -\nabla\cdot\mathbf{q} - \Pi : \nabla\mathbf{u} + Q + S_e^{rf} \quad (17)$$

In order to evaluate these quantities, it is necessary to evaluate the area- perpendicular-to-flow corresponding to a given point on a given ray in the ray bundle. Essentially, this means we are collecting information about the rays collectively as well as individually. The appearance of the ratio $P/\sigma_\perp$ in the quasilinear terms is reassuring; for a fixed volume of space, an increased ray density implies both a reduced power-per-individual-ray (assuming the total power injected remains fixed) as well as a smaller area- perpendicular-to-flow corresponding to each individual ray. By implication, convergence can be achieved as the number of rays is increased. To calculate these areas, and the quasilinear diffusion coefficients, a separate code (QLCALC) was written. QLCALC interfaces with the QHULL computational geometry package to calculate the area elements. It first takes the projection of the GENRAY ray data into a particular plane, and finds the Delaunay triangulation of the data in that plane. It then finds the outer boundary of the triangulation and reflects triangles with two vertices on this boundary about the line containing these vertices; see Figure 1 for further details. This constructs a set of "ghost points" outside the original dataset piercing the plane, bounding this dataset and ensuring that the area corresponding to the outermost rays of the GENRAY bundle will be finite. QLCALC then calls QHULL routines to find the Voronoi mesh corresponding to the original+ghost data; this mesh defines the vertices which subdivide the plane into polygons containing the set of nearest-neighbor points of the original data. The calculation of the area of these polygons is then trivial, and the area elements are obtained.

QLCALC also reads GENRAY data and correctly inserts the fields, wavenumbers, frequency, etc. into the above formula, enabling the calculation of quasilinear diffusion coefficients locally along the rays in the ray bundle. However, the data must then be interpolated to NIMROD's datastructures, which differ from the (effectively unstructured) GENRAY mesh in that NIMROD uses a finite-element, grid-based representation in the poloidal plane and a pseudospectral (Fourier) representation in the toroidal direction. The projection of the GENRAY ray bundle into NIMROD's poloidal planes, as shown in Figure 2, is resolved by NIMROD's grid without substantial difficulty. However, because the GENRAY rays may intersect the poloidal plane at points other than NIMROD gridpoints, a weighted cubic spline method (Shepard's algorithm) was used to construct a spline fit to the GENRAY data at the crossing points. The fitting function was then evaluated at NIMROD gridpoints to transfer the data into the NIMROD representation. Cubic polynomial and cosine basis functions were compared and shown to give comparable, physically reasonable results.

Toroidal resolution of the data is a somewhat more difficult prob-

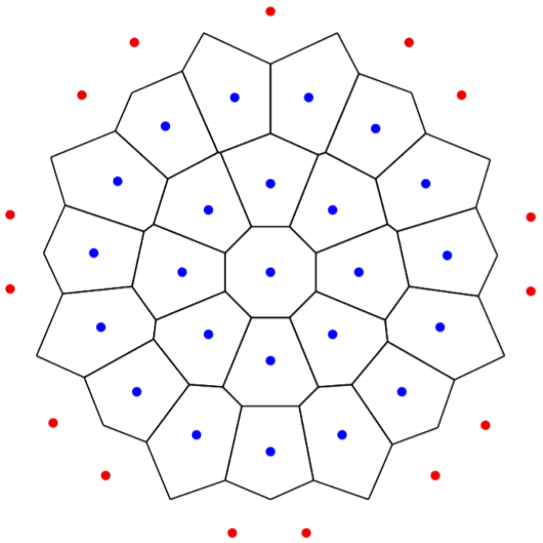

Figure 1: An example of the mesh created from the GENRAY data points (blue). Using the QHULL package, the Delaunay triangulation of this data (not shown) is constructed, and the outermost triangles are then reflected across the convex hull to form ghost points (shown in red). The Voronoi diagram (black) of the GENRAY and ghost datasets is then created, and the areas of Voronoi cells are calculated. Inclusion of ghost points ensures the finite area of the outermost Voronoi cells.

lem. NIMROD's toroidal representation effectively corresponds to a set of toroidal collocation points (planes) through which the ray bundle may or may not pass; further, the region of large quasilinear diffusion within the ray bundle may not correspond to the crossing points within the planes (see Figure 3 for details). Conventionally, NIMROD uses 32-64 modes (and thus, the equivalent number of collocation planes) for high- resolution runs; this resolution is generally adequate for the long-wavelength MHD instabilities conventionally studied in NIMROD simulations. However, adequate resolution of the data shown in the figure would require 512 modes. While this figure is within the realm of possibility, the computational cost is high; further, the wastefulness of resolving the entire torus simply for the sake of capturing a few gridpoints suggests an alternative approach. Toroidally averaging the GENRAY data and then spreading the resultant function out over the lower-resolution collocation planes should not interfere with the salient physics of tearing mode stabilization; as the modes in question [typically with helicity $(2, 1)$] have scale lengths on the order of halfway around the torus, the spreading

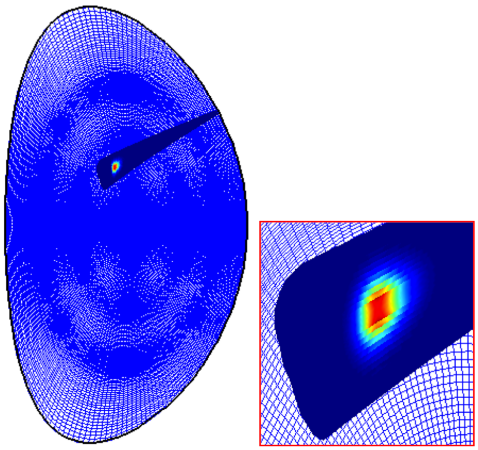

Figure 2: A plot of the magnitude of the quasilinear operator from the GENRAY ray bundle, superimposed on NIMROD's finite element mesh, shows the localized nature of the source. In the poloidal plane, the adequate resolution of the quasilinear diffusion coefficient presents little difficulty, though only a few gridpoints are affected by the diffusion.

of the GENRAY data to encompass a sixth of the torus does not seem unreasonable. More generally, one can spread according to

$$F(R,Z,\phi) = \left[\frac{1}{2\pi}\int_0^{2\pi} F(R,Z,\phi')\ d\phi'\right] g(\phi)\ ; \tag{18}$$

we have had success with functions of the form

$$g(\phi) = \frac{2\pi}{\phi_c}\cos\left(\frac{\pi(\phi-\phi_0)}{2\phi_c}\right)^2\ . \tag{19}$$

Because of NIMROD's dealiasing scheme, the function width ϕ_c must be large enough (in realspace) that the Fourier space representation is narrowed and the coefficients cut off by the dealiasing are negligibly small. Should the function be too narrow in realspace, the wide tails that result in the Fourier space are cut off, and Gibbs-like phenomena result in the ensuing realspace representation (corresponding to an unphysical induced current in undesirable regions of the simulation domain). Typically, distributions which intersect six or more poloidal planes do not suffer from these dealiasing effects.

IPS component scripts were successfully written to run GENRAY, together with QLCALC and nimset (run as a preprocessor for GENRAY to get a compatible equilibrium file), and to pass data appropriately from NIMROD to the other codes. In addition, a driver script

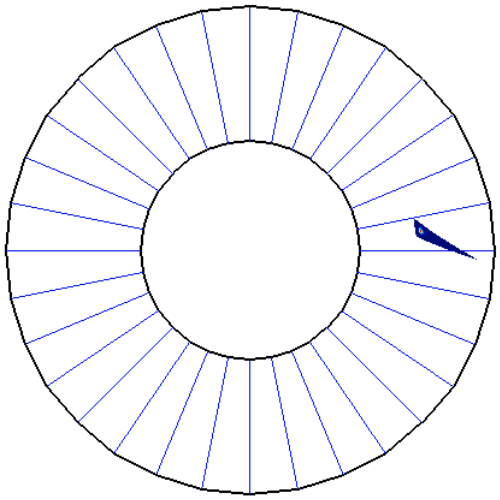

Figure 3: A plot of the magnitude of the quasilinear operator from the GENRAY ray bundle, superimposed on the poloidal planes corresponding to NIMROD's toroidal pseudospectral representation, shows the localized nature of the source. Without greatly increasing the toroidal resolution, and thus the computational cost, the data shown will not be resolved by NIMROD. The computational cost of increased toroidal resolution can be circumvented by toroidal spreading of the diffusion coefficients onto the planes shown here.

was written to control the simulation from beginning to end, running NIMROD's preprocessor, NIMROD, GENRAY, QLCALC, an IPS monitoring component, and two NIMROD plot packages simultaneously and in the correct order. The data transferred between codes has been examined and shown to be physically reasonable, with the rms energy transferred from GENRAY's ray bundle having amplitude and sign consistent with the added energy appearing in the NIMROD plasma in the presence of RF. Further, more detailed benchmarks are planned with the CQL3D code, though these will likely be deferred until the physics of RF/MHD closures can be included in the simulations in more detail. In any case, the requirements for this task have been satisfied.

(c) *Perform tearing mode simulations that explore the effect of ECCD source modulation at low plasma beta.*

This task was completed to a point, whereupon it was determined that additional work outside the scope of the task list would be necessary to enable its successful completion. Initial simulations comparing the effects of time-modulated and nonmodulated ECCD, using the *ad hoc* model for current sources, were first conducted. In Fig-

ure 4, one such simulation is shown, using a toroidally localized RF source which extends 1/10 of the way around the torus and is offset radially inward from the original rational surface by 0.05 cm. Here, magnetic energy is plotted, which can be thought of as synonymous with the width of the magnetic islands. When the unmodulated RF is introduced (dashed line), the island width decreases, first slowly and then quite sharply. However, after dipping below a certain threshold (corresponding quite well with the threshold at which islands can be detected numerically), the islands immediately grow again. This behavior can be explained by careful examination of the Poincaré plots of the islands. In Figure 5, a closeup of the Poincaré map of the plasma during the initial decrease of the mode amplitude is shown, together with the superposed full-width-half-maximum of the Gaussian source in this plane. One observes that the magnetic island, initially possessed of $(2, 1)$ helicity, is being pinched at its O-point such that the helicity becomes $(4, 2)$; the RF is introducing additional X-points through reconnection. In Figure 6, the creation of the new X-point is confirmed; this Figure shows the Poincaré map near the time of maximum $(2, 1)$ mode suppression. The suppression occurs via the $(4, 2)$ island creation; because the saturation width of the $(4, 2)$ tearing modes is considerably smaller, the mode amplitude is continually reduced (decreasing blue dashed line in Figure 4). However, after decreasing below a certain threshold, the $(2, 1)$ mode grows rapidly again with a differing toroidal phase. Essentially, the RF has demanded that an X-point occur at the injection location, and the plasma obliges by growing a $(2, 1)$ mode (a mode against which the equilibrium is unstable) around the prescribed X-point. The initial presence of the island O-point at the prescribed location means the plasma must first reduce the $(2, 1)$ island width before slipping the phase. Observations of this phase-slipping behavior were also made in early DIII-D tearing mode experiments [private communication, R. J. La Haye, 2009].

It was hypothesized that the introduction of time-varying RF as the island suppression occurred would preclude the creation of an X-point at any particular point in the plasma, and a number of numerical experiments were conducted to this end. Returning to Figure 4, the introduction of sinusoidally varying RF (within the envelope described by the RF dependence of the unmodulated simulations) was attempted but was found not to have significant influence in the suppression of already-saturated $(2, 1)$ islands (solid blue curve). Some attempts were made to adjust the sinusoidal frequency of the RF, but it became clear that more careful effort would be required than could be obtained by prespecifying the numerical behavior of the RF at the simulation outset. In addition, the motion of the rational surface (discussed earlier) necessitates the movement of the RF deposition

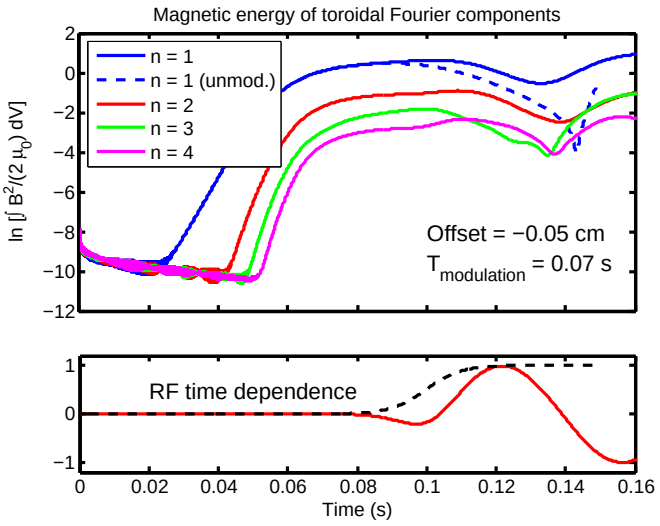

Figure 4: Time-modulated RF injection using *ad hoc* sources at the O-point of saturated islands is compared with unmodulated injection at the same location. In the unmodulated case, the mode is suppressed only temporarily due to a relocation of the island O and X-points. The presence of RF effectively demands that an X-point be created at the deposition location; from an initially saturated $(2, 1)$ island, a $(4, 2)$ island arises due to the new X-point (see Figure 5). The islands then shrink, as the $(4, 2)$ island saturation width is less than that of the $(2, 1)$ islands. Ultimately, the $(2, 1)$ mode vanishes altogether, but then regrows with an X-point at the location of the RF injection (see Figure 6), effectively slipping the phase of the X-points in the poloidal plane.

region in space as well as in time, as the islands evolve in response to the RF. To this end, it was concluded that a numerical Plasma Control system needed to be developed which could both detect the mode and calculate the RF parameters necessary for its mitigation. Such a control system is used in the DIII-D tokamak [D. A. Humphreys *et al.*, Phys. Plasmas **13**, 056113 (2006)], and to achieve fidelity with existing experiments, corresponding developments are necessary from the simulation point of view. The development of this control system will be discussed later in further detail.

2. Year 2

   (a) *Find a high-beta equilibrium which is more experimentally relevant to NTM simulations (where pressure effects, including bootstrap current terms, are important.) Begin simulations with this equilibrium.*

   This task turned out to be very difficult. Though at the time of the

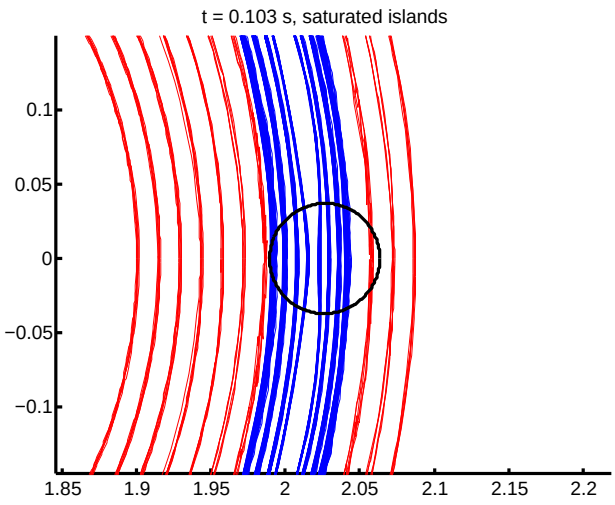

Figure 5: Poincaré mapping (with the points comprising the Poincaré section being connected for visualization purposes) of the plasma of Figure 4 when unmodulated RF sources are introduced. The source extends one-tenth of the way around the torus and has a Gaussian profile in the poloidal plane (whose full-width-half-maximum occurs at the black circle). The island contours are shown in blue and the flux surfaces in red. The RF pinches island contours inward and eventually forms an X-point at the island center (formerly occupied by the O-point; see Figure 6), thus changing the island helicity from $(2, 1)$ to $(4, 2)$ and altering the stability properties of the mode.

writing of this report it not been completed, efforts continue under the ongoing Tech-X SWIM funding. Generally speaking, the difficulties are associated with the precise definition of "experimental relevance". For instance, numerical experiments by Takahashi *et al.* [R. Takahashi, D. P. Brennan, and C. C. Kim, Nucl. Fusion **49**, 065032 (2009)] were able to successfully generate a $(2, 1)$ tearing mode with experimentally relevant values for plasma beta, but the pressure profiles associated with these equilibria vastly differed from experimentally observed profiles. In like manner, our numerical experiments with the generation of $(2, 1)$ tearing modes have been successful only when the plasma beta was extremely low, though the values for other plasma profiles have been plausible. A number of consultations with Dylan Brennan (University of Tulsa) have led to somewhat promising avenues of exploration, and it may be the case that the equilibria of Takahashi *et al.*, though dissimilar in the pressure profile, may suffice to demonstrate the relevant physics. Generally, however, the

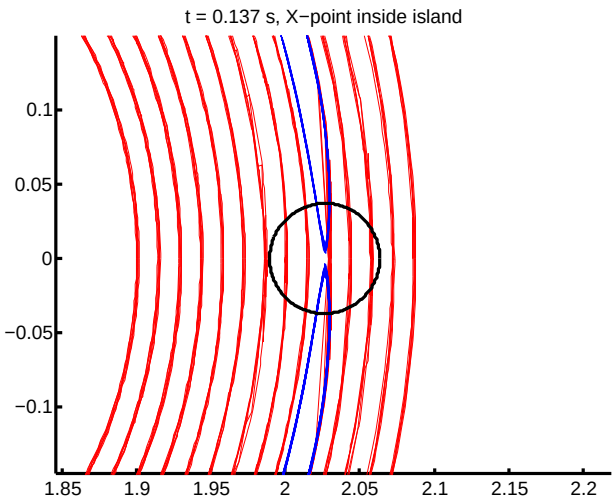

Figure 6: The eventual result of the applied RF of Figure 5 is the creation of an X-point at the point formerly occupied by the island O-point, yielding a $(4, 2)$ island in place of the original $(2, 1)$ island. The plasma is stable against $(4, 2)$ islands, and the mode consequently shrinks; the $(2, 1)$ island is then regrown with the X-point occurring at the location of the RF deposition.

onset of the tearing mode in the high-beta neoclassical regime is not well-understood. In any case, work toward an acceptable solution to the problem (in conjunction with researchers external to the SWIM project for whom the problem is also of interest) continues under the ongoing funding.

(b) *Develop a synthetic soft X-ray diagnostic for NIMROD. Perform detailed analysis of the physics of tearing mode stabilization, and compare with experimental results.*

This task was motivated by a desire to explore various methods by which data from existing plasma diagnostics could be used in the detection and mitigation/control of magnetic islands. Essentially, one wants to use the data from various diagnostics in a feedback loop, as dictated by a control system of some kind; the amplitude, spatiotemporal dependence, and type of feedback that the control system should give is determined from a study of the physics associated with the diagnostic measurements.

As has already been noted, the development of a plasma control system was determined to be a needful aspect of this research that was, nevertheless, not specified in the initial task list. Consequently, our efforts toward this particular task, rather than focusing specifically

on the development of a soft X-ray diagnostic, have centered on the development of a numerical control system as a whole. Such a system should carry out specific tasks (mode amplitude detection, spatiotemporal localization of magnetic island O-points, calculation of appropriate RF parameters by which current can be driven at these points, etc.), and these tasks should be carried out modularly (several separate approaches to accomplishing a particular task should be possible, e.g. one may detect the position of island O-points directly from the code, or by data from a synthetic diagnostic). The control system logic will depend on the output from these various tasks; ultimately, the goal is to not only suppress the magnetic islands, but to do so rapidly and efficiently by taking advantage of the available data and our knowledge of the relevant physics.

A schematic of the initial numerical Plasma Control System (hereafter PCS) is shown in Figure 7. Initially, a synthetic signal from Mirnov coils is constructed from NIMROD data. The pseudospectral representation which NIMROD uses in its toroidal direction make the construction of this signal relatively easy; B_z perturbations at a point on the outboard midplane at the plasma edge, in the Fourier representation, constitute the real and imaginary parts of the signal. In the presence of a tearing mode, a signal of the form

$$B_z(\text{outboard midplane}, n = 1) \sim Ae^{\gamma t}e^{i(\omega t+\phi)} \tag{20}$$

is obtained, where A is the mode amplitude, ω is the plasma toroidal rotation frequency (the mode rotates with the plasma), γ is the mode growth rate, and ϕ is the initial phase of the signal. Curve fits to the time history of the signal can be used to determine these parameters; once the mode amplitude rises above a certain threshold, the mode is deemed large enough to warrant intervention. The O-point of the island is found, the new input parameters for GENRAY (the RF code) are calculated, GENRAY is run, and the signal is then sent to NIMROD that the arrival of new RF data is imminent.

At this point, a number of issues should be mentioned.

- Islands rotate as the plasma rotates.
  Because of the delay between the time in which the island is detected and the time at which GENRAY has finished executing, it may not (depending on the plasma rotation frequency) necessarily be true that the island is still at the point where we have determined that RF should be deposited when NIMROD gets the new RF data. This issue can be dealt with; since the rotation frequency is known, NIMROD can be directed to wait until rotation brings the island into the deposition region again.
- O-point detection can be done via several methods, but only a few are consistent with experimental approaches.

NIMROD data can be used to calculate the location of island O-points exactly, at any time in the simulation. Experimentalists have no such recourse; rather, the position of island centers are inferred from diagnostics (e.g. motional Stark effect diagnostics, which use the splitting of emission lines via the Stark effect to determine local magnetic fields). To achieve greater fidelity with experiments, one should take both approaches in developing a numerical PCS; in addition to "seeing what the experimenter sees", we also wish to verify that the experimental interpretations of the data are correct. Consequently, our initial development of the PCS includes a routine that finds the exact locations of O-points within NIMROD data. We are also investigating methods to develop a synthetic diagnostic that more closely mirrors experimental signals associated with this aspect of mode detection.

- Islands may grow, be suppressed, and grow again.
  The PCS must account for the possibility that it will repeatedly have to turn on and off, suppressing tearing modes at various toroidal phases (and, possibly, rotation frequencies and growth rates, depending on how the plasma profiles evolve throughout the simulation) repeatedly as the simulation evolves.
- The RF signal in NIMROD must build up over a finite length of time.
  Instantaneous introduction of RF sources terms in the NIMROD equations causes numerical difficulties; new source terms must rise smoothly up from zero rather than abruptly appearing. This, however, differs little from experiments; finite ramp times for the RF power (associated with the characteristic timescales for the gyrotron power supplies) are also present there. Consequently, NIMROD has been modified to accept ON/OFF signals from the PCS, in certain cases, and to include RF data (when the ON signal is received) by ramping it up in a smooth fashion rather than by abruptly introducing it into the fluid equations. Figure 8 demonstrates the finite ramp time of the RF signal as it turns on and then off, along with corresponding mode suppression and regrowth.
- The PCS may not be able to initially hit the island O-point in cases of low rotation.
  In experimental devices, the gyrotrons which generate the RF waves operate at fixed frequencies. Because the dominant magnetic field in the tokamak is toroidal and decreases as $1/R$, where R is the major radius, the cyclotron resonance for a fixed frequency occurs on a cylindrical surface whose axis corresponds to the tokamak center stack. If toroidal plasma rotation is absent or occurs at low frequencies (as is projected to be the case in

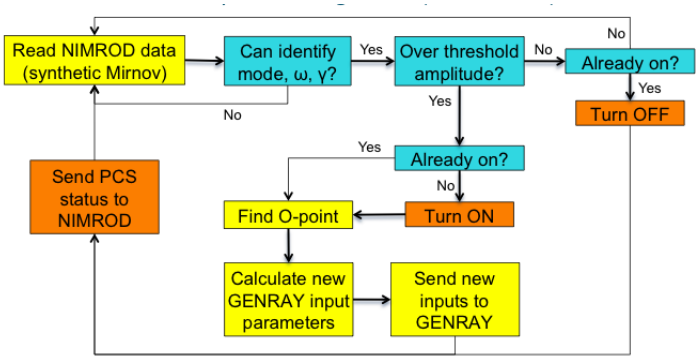

Figure 7: Schematic of the numerical Plasma Control System and its interaction with GENRAY and NIMROD in the coupled simulations.

the ITER device), it is possible for islands to grow in regions where island O-points are inaccessible to the gyrotron (i.e. the quasistationary locations of the O-points in the poloidal plane where RF is deposited may not intersect the cylindrical resonant surface).

Experimentally, this issue can be resolved by the use of resonant magnetic perturbations, which (if appropriately selected) can be used to steer the island into regions accessible by the gyrotron [F. Volpe *et al.*, Phys. Plasmas **16**, 102502 (2009)]. To simulate this technique numerically is a challenging, though not insurmountable, problem; for the moment, the use of rotating plasmas has deferred the issue.

More generally, alignment of the RF deposition with the island O-point can be accomplished by altering the plasma position within the vacuum vessel, by minor variation of the toroidal field (to change the location of the resonant surface), or by steering the RF beam using mirrors. Of these techniques, only the latter is suitable for our purposes; NIMROD would require extensive refactoring to accommodate time-varying equilibria over the course of the simulation.

Our recent work has focused on developing the PCS, with the aforementioned issues in mind, and testing it in coupled simulations to verify robustness. This work will also continue under Tech-X's SWIM funding. The soft X-ray diagnostic mentioned in the task summary is anticipated to become a component of the PCS as this development proceeds.

(c) *Perform NTM simulations with integral closures (being developed by E. Held at Utah State University).*

This task has not been completed because the development of the

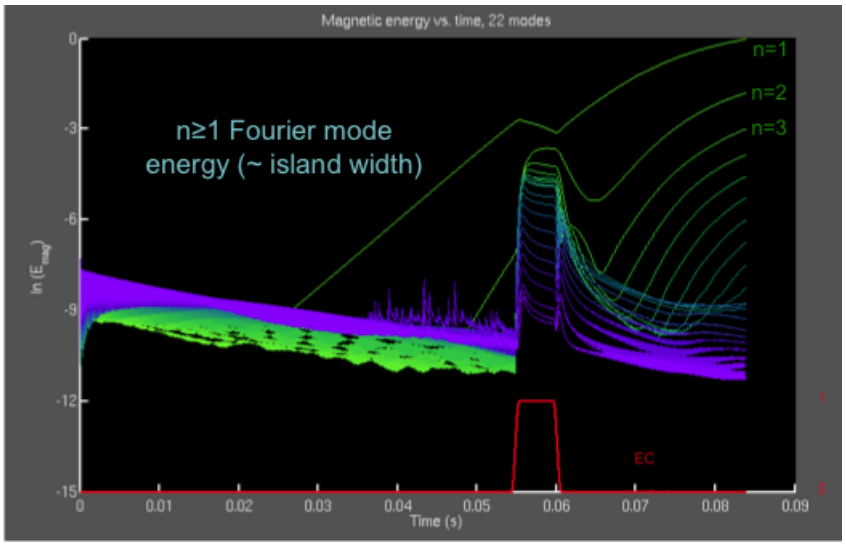

Figure 8: Logarithm of the magnetic energy of various Fourier components of the NIMROD plasma, together with the normalized amplitude of electron cyclotron power injected at the island O-point. The growth in the n=1 component of magnetic energy corresponds to $(2, 1)$ island growth. When the amplitude threshold is exceeded, the PCS detects mode parameters and injects RF at the island O-point in an effort to suppress it. The RF is ramped up according to physically reasonable timescales associated with the gyrotron power supplies. Upon suppression of the mode, the PCS turns off and the mode grows again (the PCS remains off thereafter).

integral closures has not been completed (in retrospect, this task has made unwarranted assumptions about the speed at which the closure problem could be solved, and its dependence on the efforts of unfunded SWIM participants compounds the difficulties.). Though the development of suitable RF/MHD closures is a more difficult problem than originally expected, Dr. Held has made considerable progress in the development of numerical methods to solve the relevant drift-kinetic equation. Numerical experiments to represent the kinetic distortion on velocity grids in speed and pitch-angle coordinates have been fruitful, and the development of preconditioning methods to efficiently calculate the effect of the linearized Coulomb collision operator on the kinetic distortion function has likewise met with success. In the meantime, Tech-X efforts have focused on developing a qualitative understanding of the physics that accurate closures will contribute to the problem. (The collisional friction, for instance, can be shown to depend on the electron heat flux [S. P.

Hirshman and D. J. Sigmar, Nucl. Fusion **21** (1981)] in the form

$$\mathbf{R}_{ei} = \eta \left[\mathbf{J} + \frac{3e\mathbf{q}_e}{5T_e} \right] \tag{21}$$

and thus, even in the absence of RF physics, can influence the resistivity in the Spitzer problem.) Qualitatively, the physics associated with ECCD can be categorized [G. Giruzzi *et al.*, Nucl. Fusion **39**, 107 (1999); N. J. Fisch, Rev. Mod. Phys. **59**, 175 (1987)] into three distinct effects:

- Wave-electron parallel momentum exchange. This is represented by the $\mathbf{F}_e^{rf}$ term of Eq. (16). This term drives only about a third of the total driven current of ECCD due to its resonance with the perpendicular component of the velocity. The time scale for this term is the time scale due to the gyrotron [G. S. Nusinovich *et al.*, IEEE Trans. Plasma Sci. **32**, 841 (2004)], which is on the order of $10 - 100\ \mu s$ and is dominantly determined by the time scale of the voltage supplies.
- Asymmetric collisionality. Because energy is deposited into the perpendicular component of the electron distribution function, the distortion gives an asymmetric resistivity that causes current to be driven. This is the Fisch-Boozer effect [N. J. Fisch and A. H. Boozer, Phys. Rev. Lett. **45**, 720 (1980)] and is the dominant mechanism for the current drive.
- Selective electron trapping. For resonant particles near the trapped-passing boundary, energy deposited into the electrons can cause passing electrons to become trapped, thus decreasing the total current. This is the Ohkawa effect [T. Okhawa, General Atomics Report GA-A13847 (1976)].

These terms are often termed "currents", in the same way the electron stress tensor term in the moment equation is termed the bootstrap current, because they all have collisional dependency similar to the $\eta\mathbf{J}$ term.

The Fisch-Boozer current can be described using a drift kinetic equation without the drift terms. Solutions of the kinetic distortion equation without the drift terms [E. D. Held, Phys. Plasmas **11**, 2419 (2004)] show that the dominant effect is on the parallel heat flux. This is consistent with the modifications of collisional friction occurring through heat flux modifications in the standard $\eta\mathbf{J}$ term (as seen in Eq. 21). The Ohkawa term is a modification of the trapped particle effects, and requires the inclusion of the drift terms in the drift kinetic equations to be correctly calculated. This is the drift-kinetic term required to give a correct calculation for the bootstrap current. Because the trapped particles will also reduce the parallel heat flux [E. D. Held *et al.*, Phys. Plasmas **10**, 3933 (2003)], the Ohkawa current requires the stress tensor and heat flux terms to be calculated

from a drift kinetic equation that contains the correct drift terms [J. J. Ramos, Phys. Plasmas **17**, 082502 (2010)].

We anticipate that as numerical/theoretical work on the closure problem proceeds, the increased capability of NIMROD to handle various aspects of the RF/MHD closure problem can be employed to further develop and verify our qualitative understanding of the physics. This work will continue under the present SWIM funding at Tech-X.

(d) *Collaborate with experimentalists in validating the model, such that the validity of these results and their extrapolation to ITER is well understood.*

This task is in process and will continue under current SWIM funding. We have been in contact with DIII-D personnel to discuss the operations of the control system on that device, and are using the insight gained to further develop the PCS and apply it in realistic experimental scenarios.

3 Other activities

In addition to our ongoing efforts in the development of the PCS, and our continued interaction with non-SWIM and non-funded SWIM participants (in pursuing experimentally relevant equilibria near the stability boundary for the $(2, 1)$ neoclassical tearing mode and solutions to the self-consistent RF/MHD closure problem), a number of other ongoing projects relevant to SWIM goals were accomplished during the funding period. A number of improvements to the SWIM monitoring portal interface were suggested and implemented based on the research presented herein (by SWIM personnel not directly funded under this grant), and further work relating to the visualization of data from the coupled simulations with the VisIt software has been, and continues to be, pursued in collaboration with Allen Sanderson (University of Utah). In addition, initial theoretical work generalizing the derivation of the quasilinear operator to relativistic regimes (of relevance to eventual ITER modeling) has been carried out and likewise continues under current funding.

4 Conclusion

As previously noted, the period of performance for this subcontract encompasses neither the beginning nor the end of the SWIM project, as is reflected by the as-yet- incomplete status of a number of the projects discussed herein. However, based on the information presented here, in conjunction with the proposed task list and the evolving needs and goals of the SWIM project, we believe that the work funded by this subcontract has been satisfactorily completed and that the funds expended in the pursuit of that work have been responsibly dispensed.